Title

Ykt6 SNARE protein drives GluA1 insertion at synaptic spines during LTP

Authors

Momoko Takahashi[1] and Gabriela Caraveo[1]*

[1]Department of Neurology, Feinberg School of Medicine, Northwestern University, Chicago, IL, USA
* Corresponding author

Keywords

Glutamate receptor, long-term potentiation, hippocampus, SNARE, Ykt6, ER

Abstract

Long-Term Potentiation (LTP), a crucial form of synaptic plasticity essential for memory and learning, depends on protein synthesis and the upregulation of GluA1 at postsynaptic terminals. While extensive research has focused on the role of endosomal trafficking in GluA1 regulation, the contribution of endoplasmic reticulum (ER) trafficking pathways remains largely unexplored. A key opportunity to investigate this emerged from Ykt6, an evolutionarily conserved SNARE protein and a master regulator of vesicular fusion along ER-trafficking pathways. Here, we demonstrate that Ykt6 is highly expressed in the mammalian hippocampus, where it localizes to synaptic spines and regulates GluA1 surface expression in an LTP-dependent manner. Furthermore, we found that Ykt6 modulates synaptic vesicle pool dynamics as well as the amplitude and frequency of miniature excitatory postsynaptic currents. Ykt6 loss of function has been linked to α-synuclein pathology, a hallmark of Lewy Body Dementias (LBDs), where α-synuclein misfolding in the hippocampus disrupts LTP. Taken together, our findings establish Ykt6 as a critical SNARE protein in hippocampal function during LTP, with significant implications for neurodegenerative disorders such as LBDs.

Introduction

Through an unbiased phosphoproteomic approach, our laboratory previously identified Ykt6 as a substrate of the Ca^{2+}-dependent serine/threonine phosphatase, calcineurin (CaN) (1). Ykt6, an essential soluble N-ethylmaleimide-sensitive factor attachment protein receptor (SNARE), regulates vesicular fusion along the secretory pathway, namely the transport between the endoplasmic reticulum (ER) and Golgi apparatus, within the Golgi, from the Golgi to the plasma membrane (2, 3), and in autophagy-related vesicular fusion pathways (1, 4–10). Unlike most SNARE proteins, Ykt6 lacks a transmembrane domain and relies on reversible lipidation for recruitment to membranes to facilitate vesicular fusion. We and others have established that in the inactive state, Ykt6 is localized in the cytosol in a close conformation, whereby the regulatory longin domain is closely associated with the SNARE domain (1, 3, 10–12). In the active state, phosphorylation at the SNARE domain builds up the electrostatic potential which causes an intra-conformational change separating the longin and the SNARE domain enabling C-terminus lipid modifications (1, 11, 13–17). Reversible lipidation allows Ykt6 to be anchored to the ER, Golgi and plasma membranes (1, 13, 14, 16, 18, 19). Our laboratory also discovered that the subsequent dephosphorylation of the SNARE domain by CaN enhances SNARE-SNARE protein interactions, thereby facilitating vesicular fusion in both the secretory and autophagic pathways (1).

At excitatory synapses, α-amino-3-hydroxy-5-methyl-4-isoxazolepropionic acid receptors (AMPARs) modulate synaptic strength to facilitate information processing and storage (20–23). AMPARs are rapidly inserted into synapses during long-term potentiation (LTP), a form of synaptic strengthening (24). While the roles of exocytosis and endocytosis in activity-dependent AMPAR transport at postsynaptic terminals are well-established (25–29), little is known about the contribution of activity-dependent roles of the secretory pathway. GluA1, an AMPAR subunit, is a good candidate for studying secretory transport in relation to synaptic plasticity in hippocampal neurons. First, GluA1 as the rest of AMPAR subunits, are synthesized in the ER where they assemble to form the channel (30–32). Second, GluA1A2 heteromers are the predominant AMPA receptor type that mediates synaptic transmission in the hippocampus (33–35). Third, while GluA2 localizes around the plasma membrane and remains relatively static, GluA1 relies more on local protein synthesis and activity-dependent trafficking for constant transport to the synaptic space (36–38). Lastly, synaptic insertion of GluA1-containing AMPARs is necessary for LTP (39–46).

LTP triggers Ca^{2+} influx through both N-methyl-D-aspartic acid receptors (NMDARs) and AMPARs, and our previous findings in yeast and HeLa cells demonstrated that Ykt6 activity is regulated by CaN (1), whose activity is dependent on Ca^{2+}. Moreover, we and others have implicated Ykt6 loss of function in α-synucleinopathies, neurodegenerative diseases characterized by deficits in LTP (1, 47–49). Therefore, we asked whether Ykt6, the master regulator of the secretory pathway, participates in delivering GluA1 subunits at synaptic terminals during LTP. Here we show that Ykt6 is highly expressed in the hippocampus in the mammalian brain. Using primary pyramidal hippocampal neurons, we demonstrate that Ykt6 relocates to synaptic spines in response to LTP and promotes surface expression of GluA1. Moreover, we show that Ykt6 regulates the number of synaptic vesicular pools, the amplitude and frequency of miniature excitatory

postsynaptic currents. Taken together, our findings highlight a critical role for Ykt6 in LTP with implications to α-synucleinopathies.

Results

Ykt6 is highly expressed in the mammalian hippocampus

We first began by examining Ykt6 expression in the mammalian brain using the human and mouse brain atlas (50, 51). In the human brain, data from six subjects who were otherwise healthy at the time of death was available. We examined Ykt6 expression using two different mRNA probes targeting Ykt6 in different brain regions, including the hippocampus. As a reference control, we analysed the expression of the neuronal specific microtubule associated protein 2 (MAP2), a highly expressed neuronal protein. Relative to MAP2, the highest expression of Ykt6 was in the globus pallidus followed by the hippocampus (Figure 1A, hippocampal formation). In the rodent brain, while the mRNA probe for Ykt6 was ubiquitously expressed throughout the brain, its expression was highest in the hippocampus and cerebellum, followed by the frontal cortex (Figure 1B). Together, these data show that under physiological conditions Ykt6 is highly expressed in the mammalian hippocampus (52–64).

At rest, Ykt6 is mainly cytosolic, with some colocalization with the Golgi apparatus and ER at somatic and dendritic terminals in hippocampal neurons.

We next examined the intracellular localization of Ykt6 in rat primary hippocampal neurons in culture using immunofluorescence. In resting conditions, Ykt6 was primarily cytosolic in both the somatic and dendritic regions (Figure 2A-D,I-L). Consistent with its role in the secretory pathway (65), Ykt6 also localized to the Golgi apparatus and to the ER, as shown by the colocalization with the Golgi marker GM130 and the ER-resident protein disulfide isomerase (PDI) (Figure 2A-D,I-L). Ykt6 localization is specific, as reducing endogenous Ykt6 expression with a lentivirus expressing an inducible ShRNA targeting Ykt6 to knock down its expression (Sh Ykt6) significantly diminished Ykt6 detection compared to neurons expressing a scramble ShRNA sequence as a control (Sh Ctrl) (Figure 2E-H,M-P). Together, these data indicate that under resting conditions, Ykt6 is primarily cytosolic but also associates with the ER and Golgi apparatus at somatic and dendritic locations.

Ykt6 mobilizes to synaptic spines in a cLTP-dependent manner

Next, we investigated whether Ykt6 is present at postsynaptic spines in hippocampal neurons. To address this, we analysed its localization using immunofluorescence relative to postsynaptic density protein 95 (PSD-95), a standard postsynaptic marker, and performed subcellular fractionation for biochemical assessment. At resting conditions, Ykt6 was present at postsynaptic spines as demonstrated by immunofluorescence through colocalization with the postsynaptic marker PSD95 (Figure 3A,B), and biochemically by its increased expression in the synaptosomal fraction (Figure 3C,D). We then asked whether the induction of chemical long-term potentiation (cLTP) with glycine, a widely used method to enhance synaptic plasticity at postsynaptic spines (66–71), affects Ykt6 localization. As reported by many others (72), cLTP treatment increased GluA1 expression at postsynaptic spines (Figure 3C,E). Interestingly, the induction of cLTP also increased Ykt6 expression at postsynaptic spines, as assessed by immunofluorescence, which showed colocalization with the

postsynaptic marker PSD-95 (Figure 3A,B). This finding was further supported biochemically by its increased expression in the synaptosomal fraction (Figure 3C,D). Together, these data indicate that while Ykt6 is present at postsynaptic spines under resting conditions, it is further mobilized to postsynaptic spines upon cLTP induction.

Ykt6 regulates GluA1 expression at synaptic spines in a cLTP-dependent manner

Modulation of the synaptic distribution of AMPARs underlies synaptic plasticity (20–23). In addition, AMPAR subunit assembly occurs within the ER (31, 32, 73, 74). Therefore, ER transport of AMPA receptors may modulate the synaptic pool available for membrane insertion, thereby impacting synaptic plasticity. Among the four AMPARs subunits (GluA1-4), GluA1 is a good candidate for studying secretory transport in relation to synaptic plasticity in hippocampal neurons. In the hippocampus, synaptic transmission is primarily mediated by GluA1A2 heteromers (33, 34). While GluA2 remains relatively stable near the plasma membrane, GluA1 depends on continuous intracellular trafficking to reach the synaptic space. Moreover, the synaptic insertion of GluA1-containing AMPARs is necessary for LTP (33, 39–46, 71, 75). To test if Ykt6 affects the distribution of endogenous AMPARs, we performed immunocytochemistry for surface and internal GluA1 on pyramidal neurons from the primary rat hippocampal cultures. The surface-to-internal ratio indicates that the regulation primarily occurs at the plasma membrane level rather than reflecting a global change in GluA1 expression. Primary hippocampal rat neurons were co-transduced with lentiviruses expressing an inducible ShRNA targeting Ykt6 to knock down its expression (hereafter referred to as Ykt6 knock down), or a scramble ShRNA sequence as a control (hereafter referred to as control). Additionally, an N-terminally green fluorescent protein (GFP) tagged human Ykt6 (GFP-Ykt6 WT), resistant to the Ykt6 ShRNA, was co-expressed to rescue Ykt6 expression to endogenous levels or GFP alone was used as control. Western blot analysis confirmed that Ykt6 knockdown reduces endogenous Ykt6 expression by approximately 70% and that the GFP-Ykt6 WT resistant construct successfully restores Ykt6 expression to endogenous levels (Figure 4A,B).

Under resting conditions, Ykt6 knockdown slightly reduced surface expression of GluA1 compared to the control (Figure 4C,D). Overexpression of GFP-Ykt6 WT however, did not further increase surface GluA1 levels under basal conditions compared to control condition (Figure 4C,D), suggesting that GluA1 regulation is tightly controlled at rest. The effect on GluA1 surface levels under basal conditions was specific to Ykt6, as co-expression of a Ykt6 knockdown-resistant construct restored basal surface GluA1 levels (Figure 4C,D). As previously reported (72), cLTP treatment led to a two-fold increase in GluA1 surface expression under control conditions (Figure 4C,D, grey bars). Conversely, Ykt6 knockdown prevented the cLTP-induced increase in GluA1 surface expression (Figure 4C,D purple bars). Importantly, this effect was specific to Ykt6, as restoring endogenous Ykt6 expression with a knockdown-resistant construct reinstated the two-fold increase in surface GluA1 levels following cLTP treatment, similar to control conditions (Figure 4C,D blue bars). While overexpression of GFP-Ykt6 WT further increased surface GluA1 levels compared to the control under cLTP conditions, this effect was not statistically significant (Figure 4C,D green bars). Collectively, these findings indicate that Ykt6 regulates both basal and cLTP-dependent surface GluA1 levels.

Ykt6 modulates both pre- and post-synaptic terminals of glutamatergic neurotransmission

Given the evidence that Ykt6 modulates synaptic connections and their downstream effects, we conducted whole-cell patch-clamp electrophysiology to measure miniature excitatory post-synaptic currents (mEPSCs) in pyramidal hippocampal neurons, providing further insight into synaptic dynamics. Rat primary pyramidal hippocampal neurons transduced with Sh Ctrl or Sh Ykt6 were patched and recorded in the presence of NMDA receptor blocker D-2-amino-5-phosphonopentanoic acid (D-APV), voltage-gated sodium channel blocker tetrodotoxin (TTX), and Gamma-Aminobutyric acid (GABA) subunit A ($GABA_A$) receptor antagonist picrotoxin (PTX) to isolate AMPA-mediated currents. Ykt6 knockdown reduced the amplitude of mEPSCs compared to the control without significantly changing the distribution of the mEPSC amplitudes (Ykt6 Knockdown, 8.728 ± 0.486pA, control, 10.64 ± 0.400pA, p = 0.009, unpaired T-test) (Figure 5A,B). The observed reduction in mEPSC amplitude aligns with the decrease in GluA1 surface density at the postsynaptic site that we observed by immunofluorescence (Figure 4C,D). Moreover, we detected a concordant decrease in the interevent cumulative percentage (Figure 5C; D= 0.595, p < 0.0001) and the frequency of interevent intervals in Ykt6 knockdown (0.357 ± 0.037 Hz) compared to the control (0.750 ± 0.010 Hz) (Figure 5D, p= 0.003, unpaired T-test with Welch's correction). Importantly, the decrease in mEPSCs is not due to neuronal viability issues, as ATP levels—a reliable indicator of cell viability—remained unaffected by Ykt6 knockdown (Figure 5F).

To investigate whether the changes in synaptic transmission were due to changes in the number of vesicles associated with the synapse, we performed electron microscopy (EM) on rat primary pyramidal hippocampal neurons transduced with Sh Ctrl or Sh Ykt6. In line with previous studies (76, 77), we classified the vesicles that are touching synaptic contact points as the readily releasable pool (RRP), those proximal to the contact point but not touching membranes as recycling pool, and those distal from the contact point as reserve pool. Ykt6 knockdown exhibited spines with an immature filopodia-like morphology, whereas the control spines displayed a characteristic mature mushroom-like shape (Figure 5G). Furthermore, Ykt6 knockdown resulted in fewer synaptic vesicles in both the readily releasable pool (RRP) and the reserve pool, while the distal pool remained unaffected (Figures 5H–J). Additionally, we observed a slight increase in the average size of synaptic vesicles across all three pools in the Ykt6 knockdown condition (Figure 5K). Together, these data indicate that Ykt6 regulates the RRP, ultimately impacting mEPSC synaptic function in pyramidal hippocampal neurons.

Ykt6 regulates dendritic arborization

The secretory pathway is not only important for neurotransmitter release and synapse morphology, but it also provides proteins essential for dendritic morphogenesis (97, 98). Dendritic arborization is crucial not only during neurodevelopment but also in adult neurons, where synaptic activity can influence the morphology of the dendritic arbor (39, 46, 78–83). To investigate whether Ykt6's role in the secretory pathway affects dendritic morphology, hippocampal primary neurons transduced with either ShYkt6 or ShCtrl were transfected with

mCherry to visualize the dendritic arbor and analyzed at DIV21 using Sholl analysis to assess branching complexity (84). Ykt6 knockdown reduced dendritic arbor branching in pyramidal hippocampal neurons compared to the control, particularly in regions distant from the soma (Figure 6A-C). Together, these data indicate that Ykt6 also plays critical role in the regulation of the dendritic arbor.

Discussion

Ykt6's role in vesicular trafficking has been well studied in yeast and mammalian systems, yet its physiological function in the brain remains largely unknown. Here, we show that Ykt6 is highly expressed in the mammalian hippocampus. In hippocampal pyramidal neurons, Ykt6 is associated with secretory organelles, ER and Golgi (105), and can be mobilized to postsynaptic terminals upon cLTP induction. Furthermore, we demonstrate that Ykt6 regulates both basal and cLTP-dependent surface GluA1 levels, modulating the availability of vesicular pools at the synapse and ultimately impacting mEPSCs, synapse structure, and dendritic morphology in pyramidal hippocampal neurons. Reductions in GluA1 expression may result from the presence of immature spines (85) which are also observed with the loss of Ykt6. Downregulation of Ykt6 not only disrupts GluA1 trafficking to the surface, reducing synaptic amplitude, but also contributes to longer inter-event intervals. These prolonged intervals have been linked to impairments in the readily releasable pool (86) and may also result from decreased spine density and the presence of immature spines (87, 88)—all of which we observe under Ykt6 deficiency.

Ykt6 is an essential R-SNARE protein with established roles in three key vesicular trafficking pathways: the secretory, exocytosis and autophagy pathways (1, 4–8, 10, 14, 15, 19, 89–95). Our findings suggest a novel role for Ykt6 in regulating AMPARs via the secretory pathway, distinct from its roles in autophagy or exocytosis. This hypothesis is supported by the following evidence. While surface expression of AMPARs can be modulated by autophagy in an activity-dependent manner (96–101), autophagy primarily facilitates the degradation of these receptors. In contrast, our data demonstrate that Ykt6 has a positive role in both basal and activity-dependent AMPAR trafficking, enhancing receptor surface expression rather than contributing to their degradation.

The R-SNARE VAMP2 (Synaptobrevin-2) plays a crucial role in forming well-established SNARE complexes, such as SNAP25–Syntaxin-1A/B–VAMP2 or VAMP2–Syntaxin-3–SNAP-47, which are essential for AMPAR exocytosis and endocytosis at postsynaptic terminals (102–108). Although Ykt6, another R-SNARE, could theoretically substitute for VAMP2 in these complexes, it remains unclear how Ykt6 might displace VAMP2 from its known binding partners. This suggests that Ykt6 is unlikely to regulate GluA1 surface expression via exocytosis.

Neurons have evolved specialized ER and Golgi outposts at distal locations from the soma to enable rapid and precise delivery of protein cargo to synapses (109, 110). Extensive networks of smooth ER tubules and sheets in dendrites and spines suggest local secretory trafficking, bypassing traditional somatic secretory pathways (28, 81, 111–116). ER exit sites (ERES) and COPII subunits have been observed at both proximal and distal

dendritic locations in hippocampal neurons (112, 117, 118). Similarly, Golgi outposts in dendritic and axonal compartments support localized secretory functions essential for synaptic plasticity and neuronal responses. Local AMPAR synthesis in dendrites has been observed to rely on the ER-Golgi intermediate compartment (ERGIC) (119–121). Moreover, recent evidence suggests alternative sources of AMPAR synthesis coupled to synaptic plasticity-dependent signals (22, 122, 123). For example, in Drosophila, intra-Golgi transport is regulated by Ca^{2+}-calmodulin-dependent kinase II, an enzyme activated during long-term potentiation (LTP) (124–127). Additionally, the dendritic ER plays a critical role in long-term depression (LTD), a form of synaptic plasticity. During LTD, ER Ca^{2+} release is enhanced, NMDAR trafficking is upregulated, and the ER network near spines becomes more The fact that Ykt6 is present at ER and Golgi outposts in secondary dendrites under basal conditions, and relocalizes to synaptic terminals upon cLTP induction, suggests a potential role of Ykt6 in distal secretory outposts. Understanding how Ykt6 regulates AMPAR secretory trafficking at distal secretory outposts will be crucial for elucidating its molecular mechanisms and functional significance, particularly in the context of neuronal plasticity and synaptic function.

Misfolding of α-synuclein leads to a group of neurodegenerative diseases collectively known as synucleinopathies, which includes Dementia with Lewy Bodies and Parkinson's Disease Dementia (128–133). A block in ER-to-Golgi transport and a loss of Ykt6 function is a hallmark of α-synuclein pathology across various model systems (1, 4, 5, 17, 134, 135). Previous findings from our laboratory demonstrated that α-synuclein ER-to-Golgi trafficking deficits leads to a pathological increase in cytosolic Ca^{2+} levels and constitutive activation of the phosphatase CaN, leading to Ykt6 constitutive dephosphorylation and loss of function (1). Moreover, other groups have shown that α-synuclein disrupts AMPAR and NMDAR surface levels at synapses, impairing LTP and spatial learning (47, 49, 58, 136–138). Consistent with these findings, here we have shown that physiological Ykt6 loss of function in the hippocampus results in defects in both basal and cLTP-dependent GluA1 surface expression levels. Therefore, our data can provide a mechanistic explanation for how α-synuclein disrupts AMPAR trafficking and synaptic plasticity. Dysregulated AMPAR surface-level regulation has been implicated not only in Parkinson's disease but also in other neurodegenerative disorders associated with cognitive and memory deficits, such as Alzheimer's disease (122, 139–149), as well as a range of neurodevelopmental and psychiatric conditions. Therefore, our findings on the novel role of Ykt6 in AMPAR regulation within the hippocampus may open new therapeutic avenues for devastating neurological diseases.

Experimental Procedures

Primary Hippocampal Cultures

Embryonic rat hippocampal neurons were isolated from euthanized pregnant Sprague–Dawley rats at embryonic day 18 using a modified protocol from Lesuisse and Martin. Protocol was approved by Northwestern University administrative panel on laboratory animal care. Embryos were harvested by Caesarean section and hippocampi were isolated and dissociated with 0.25% Trypsin without EDTA (Invitrogen, 15090-046) digestion for 15 min at 37°C and trituration with 1 ml plastic tip. Poly-D-Lysine (Sigma, P-1149)-coated 1.5 coverslips

(Neuvitro, GG-12--1.5-oz) in 24-well plates were seeded with 5 x 10^5 cells accordingly in neurobasal medium (Gibco, 21103-049) supplemented with 10% heat-inactivated FBS (Gibco), 0.5 mM glutamine (Gibco), penicillin (100 IU/mL), and streptomycin (100 µg/mL) (Gibco). Before seeding, cells were counted using the automated cell counter TC10 (Bio-Rad) and viability (90-95%) was checked with Trypan Blue Stain (0.4%, Gibco 15250-061). After 1 hour (h) incubation at 37°C, media was changed to neurobasal medium (Gibco, 21103-049) supplemented with B27 (Gibco, 17504-044) and 0.5 mM glutamine. One half (out of 500 µl volume for 24-well plates) of the media was changed on DIVs 5, 9, 12, 16, and 19.

Plasmids

Nontargeting ShRNA (Horizon Discovery Dharmacon, VSC11656) or ShRNA targeting Ykt6 (Horizon Discovery Dharmacon, V3SH7669) were expressed in mammalian cells using lentiviral induction at DIV 5.

Expression was verified visually by the expression of turboRFP.

Human eGFP-Ykt6 (a kind gift from Dr. Joseph Mazzulli, Northwestern University) and eGFP were expressed in mammalian cells using lentiviral induction at DIV 5 at half the MOI used with ShRNAs.

Doxycycline treatment of cultures

Primary hippocampal cultures that were infected with either nontargeting ShRNA or ShRNA targeting Ykt6 were treated with doxycycline. Targeted silencing of Ykt6 in primary hippocampal cultures was induced using doxycycline treatments at a concentration of 1nM at DIV8, 12, 15, and 19 before used for experiments. Viral MOI and doxycycline titrations were performed on new batches before applied experimentally and confirmation of knockdown and expression of turbo RFP was regulated.

Chemical LTP induction

The samples were washed once with warmed extracellular solution (ECS) containing (in mM): 150 NaCl, 2 $CaCl_2$, 5 KCl, 10 HEPES, 30 Glucose, 0.001 TTX, 0.01 strychnine, and 0.03 picrotoxin at pH 7.4, then exposed to 300µM glycine in ECS for 3 minutes (external/internal staining) or 6 minutes (western blot) at room temperature, then washed with extracellular solution thrice, then incubated at 37°C for 20 minutes prior to further processing.

External/Internal Staining

External and internal glutamatergic receptors were stained according to the protocol by Chiu. et.al (72). Coverslips with primary hippocampal cultures were transferred to parafilm-covered dishes and incubated in primary antibody (GluA1: Invitrogen, MA5-27694; GluN1: Alomone Labs, AGC-001) at the concentration of 1:100 diluted in conditioned media for 15 minutes at room temperature, then washed three times with warm conditioned media. The coverslips were then washed once with phospho-buffered saline (PBS) supplemented with 1mM $MgCl_2$ and 0.1mM $CaCl_2$ (PBS+). The cells were then fixed by incubating with fresh 4% paraformaldehyde (PFA) and 4% sucrose in PBS for 8 minutes. The cells were then washed three times with PBS, then blocked with 10% normal goat serum (NGS) in PBS for minimum 30 minutes at room temperature.

The cells were then incubated with 1:400 dilution of goat anti-mouse Alexa Fluor® 405 secondary antibody (Invitrogen, A-31553) or goat anti-rabbit Alexa Fluor® 405 secondary antibody (abcam, ab175652) in 3% NGS in PBS for 1 hour at room temperature. The cells were then washed 3 times with PBS.

For internal staining, the cells were then permeabilized with 0.25% Triton X-100 (Thermo Fisher Chemicals, A16046.AP) for 7 minutes at room temperature, then blocked with 10% NGS in PBS for minimum 30 minutes at room temperature. The intracellular receptors were then labelled by incubating the cells with the same primary antibodies at the same concentration, and anti-microtubule-associated protein 2 (MAP2) chicken antibody (abcam, ab318993) at 1:10000 dilution, but diluted in 3% NGS in PBS overnight in 4°C. The next morning, cells were washed 3 times with PBS, then labelled with goat anti-mouse Alexa Fluor® 647 secondary antibody (Invitrogen, A-21235) or goat anti-rabbit Alexa Fluor® 405 secondary antibody (Invitrogen, A-21245) at 1:1000 dilution and goat anti-chicken Alexa Fluor® 488 secondary antibody (Invitrogen, A-11039) at 1:400 dilution in 3% NGS in PBS for 1 hour at room temperature. The cells were then washed 3 times with PBS and once with de-ionized water, then mounted using Prolong Gold antifade mountant (Invitrogen, P36930). The cells were imaged using Nikon A1R GaAsP point-scanning laser confocal microscope using 63x oil-immersion objective (NA = 1.4) with z-series of 10-20 images, taken at 0.3 µm intervals, with 2048x2048 pixel resolution. Only cells positive for MAP2 were acquired. The external to internal expression ratio was calculated for the basal condition with GFP and Sh Ctrl, or Sh Ctrl only. This value was then normalized to 1, and all other ratios normalized to the basal condition.

Ykt6 Staining

Primary hippocampal cultures as described above at DIV21 were washed once with PBS+, then fixed with fresh 4% PFA and 4% in sucrose in PBS for 20 minutes at room temperature. They were then permeabilized with 0.3% Triton-X 100 in PBS for 30 minutes at room temperature. The cells were blocked with 0.3% Triton-X 100/2% bovine serum albumin (BSA)/5% NGS in PBS for 30 minutes, then incubated for 48 hours at with mouse v-SNARE Ykt6p antibody (Santa Cruz, sc-365732), rabbit anti-Ykt6 primary antibody (abcam, ab236583), purified mouse anti-GM130 primary antibody (BD Biosciences, 610822) at 1:200 dilution, or rabbit anti-PDI primary antibody (Cell Signaling Technology, 3501), all at 1:100 dilution in the blocking buffer. Anti-microtubule-associated protein 2 (MAP2) chicken antibody (abcam, ab318993) at 1:10000 dilution was used to identify neurons. For PSD95, mouse anti-PSD95 primary antibody (Invitrogen, MA1-045) was used at 1:400 dilution.

After primary incubation, cells were washed three times with 0.05% Tween-20 in PBS for 15 minutes each, then with PBS twice for 15 minutes each, then incubated with then labelled with goat anti-mouse Alexa Fluor® 647 secondary antibody (Invitrogen, A-21235) or goat anti-rabbit Alexa Fluor® 405 secondary antibody (Invitrogen, A-21245) at 1:5000 dilution and goat anti-chicken Alexa Fluor® 488 secondary antibody (Invitrogen, A-11039) at 1:400 dilution in the blocking buffer for 2 hour at 4°C. The coverslips were then washed three times with 0.05% Tween-20 in PBS for 15 minutes each, and then twice in PBS for 15 minutes each, and mounted with Prolong Gold Antifade mountant. The cells were imaged using Nikon A1R GaAsP point-scanning

laser confocal microscope using 63x oil-immersion objective (NA = 1.4) with z-series of 10-20 images, taken at 0.3 µm intervals, with 2048x2048 pixel resolution. Only cells positive for MAP2 were acquired.

Sholl Analysis

Scholl Analysis was performed in cultured rat primary hippocampal cultures. Neurons were plated and allowed to mature until DIV21 and transfected with PGK-mCherry using Lipofectamine 2000 according to manufacturer's protocol at DIV 16. At DIV21 they were washed once with PBS+, fixed with fresh 4% PFA and 4% in sucrose in PBS. They were then permeabilized with 0.3% Triton-X 100 in PBS for 7 minutes at room temperature, blocked with 3% NGS in PBS, and then stained with anti-mCherry primary antibody (Abcam ab167453) at the concentration of 1:400 diluted in 3% NGS in PBS. overnight in 4°C.

The next day, the coverslips were incubated with Goat Anti-Rabbit Alexa Fluor® 594 secondary antibody (abcam, ab150080) at 1:500 concentration diluted in 3% NGS in PBS, washed 3 times with PBS, and then mounted using Prolong Gold Antifade mountant. Isolated neurons were imaged using Nikon A1R GaAsP point-scanning laser confocal microscope using 63x oil-immersion objective (NA = 1.4) with z-series of 8–10 images, taken at 0.3 µm intervals, with 1024 × 1024 pixel resolution. The stacks were then flattened to 1 image in ImageJ and Scholl Analysis performed using the SNT plugin (ImageJ)(150) after manual tracing.

Ykt6/Organelle Analysis

To measure the relative intensities of Ykt6 and the respective organelles, ImageJ was used with the ColorProfiler plugin. For the soma, a line was drawn in between the beginnings of the basal dendrites of the hippocampal neurons. For the dendrites, the line was drawn across the width of the secondary dendrite, immediately after the bifurcation point.

PSD95 distance measurement

To measure the distance between post-synaptic density 95 (PSD95) puncta and its most proximate Ykt6 puncta, coverslips were incubated per protocol above using the mouse anti-PSD95 and the rabbit anti-Ykt6 antibodies at given concentrations. The coverslips were imaged on Nikon AXR point-scanning laser confocal microscope using 100x (NA=1.49), with 2048x2048 pixel resolution and Nyquist. The images were analysed using ImageJ (84) and Colocalization by Cross Correlation package by McCall (151), by first constructing a mask to extrapolate the secondary dendrite, and then calculating the mean of all numerical values of the shortest distance of all PSD95 puncta with Ykt6 puncta.

Synaptosomal Fractionation

Synaptosomal fractionation was performed following a protocol adapted from Bermejo et.al (152). Adult brains were extracted in accordance with Northwestern University administrative panel on laboratory animal care post-decapitation. The brain was chopped with a razor blade and washed with ECS once before the glycine treatment. The brain was then snap frozen with liquid nitrogen until further processing.

The fractionation was performed as follows: solutions shown in table below were chilled, and HALT protease/phosphatase inhibitor (Thermo Scientific, 78440) was added at 1:100 dilution to all solutions.

Solutions	HEPES-buffered sucrose
1M HEPES pH 7.4	0.32M sucrose in 4mM HEPES (pH 7.4)
4mM HEPES pH 7.4	0.8M sucrose in 4mM HEPES (pH 7.4)
ddH_2O	1.0M sucrose in 4mM HEPES (pH 7.4)
540mM HEPES pH7.4/2mM EDTA	1.2M sucrose in 4mM HEPES (pH 7.4)

Table 1. Reagents for synaptosomal fractionation.

All samples and solutions were kept on ice during the procedure. The tissue was placed in a dounce homogenizer along with 1mL of 0.32M HEPES-buffered sucrose solution and homogenized with the motor drive set at 900rpm (setting 7) over 30 second period with 12 strokes. The homogenizer was rinsed with deionized water and wiped dry with Kimwipes in between samples. 10µL of homogenate was preserved and diluted to 4 times the concentration using 0.32M HEPES-buffered sucrose solution, then stored at -80°C for subsequent protein quantification and western blot analysis of the total protein fraction.

The remaining homogenate was centrifuged in a fixed angle rotor at 900xg for 10 minutes at 4°C. The supernatant (S1) was transferred to a clean Eppendorf tube, while the nuclear fraction (P1) was resuspended in 500µL of 0.32M HEPES-buffered sucrose and stored at -80 °C and used for western blot analysis of the nuclear fraction.

S1 was then centrifuged at 10,000xg for 15 minutes at 4°C. The supernatant (S2) was removed and stored at -80 °C. The pellet (P2) was resuspended in 1mL of 0.32M HEPES-buffered sucrose solution and centrifuged at 10,000xg for 15 minutes at 4°C. The supernatant (S2') was removed and stored at -80 °C for subsequent protein quantification and western blot analysis of the cytosolic/light membrane fraction.

The pellet was then lysed by resuspending it in 1mL of ddH_2O, transferred to a glass-Teflon tissue homogenizer, and rapidly homogenized by hand with 3 strokes. The sample was quickly adjusted to 4mM HEPES with 4µL of 1M HEPES solution, then returned to an Eppendorf tube, and the samples were then rotated at 4°C for 30 minutes to complete the lysing.

The sample was then centrifuged at 21,700xg for 24 minutes at 4°C. The supernatant containing the crude vesicular fraction (S3) was stored in -80°C, and the pellet was resuspended in 0.32M HEPES-buffered sucrose solution. The discontinuous sucrose gradient was prepared in 4mL open top thinwall ultra-clear tube (Beckman Coulter, 344062) by layering 1mL each of 1.2M HEPES-buffered sucrose solution, followed by 1.0M HEPES-buffered sucrose solution, then 0.8M HEPES-buffered sucrose solution using a P1000 pipette. Finally, the sample was layered on top, and the tubes were balanced using P200 pipette and adding 0.32M HEPES-buffered sucrose solution onto the top layer. The samples were then ultracentrifuged for 2 hours at 4°C in swinging buckets (Beckman Coulter, SW-60Ti) using Optima XE-90 ultracentrifuge (Beckman Coulter). Using an 18G needle and a 1mL syringe, the tubes were then punctured at the 1.0M/1.2M HEPES-buffered sucrose solution interphase and the band (synaptic plasma membrane layer, SPM) was withdrawn. The volume was noted, and the collected layer was placed in 3.5mL thickwall ultracentrifuge tubes (Beckman Coulter, 349622)

and 2.5 times the volume of SPM of 4mM HEPES was added to adjust the sucrose concentration from 1.2M to 0.32M. The tubes were then balanced with 0.32M HEPES-buffered sucrose solution, and the samples were ultracentrifuged in the swinging bucket rotor at 200,000xg for 30 minutes at 4°C. The supernatant was discarded, and the pellet was resuspended in 100µL of 50mM HEPES/2mM EDTA solution, then stored in -80 °C until used for western blotting.

Western Blot

Protein concentration was analyzed with the Pierce BCA Protein Assay kit (Thermo Scientific, 23225). After the addition of the appropriate amount of the 6X Laemmli Sample Buffer (Bio-rad sab03-02) with 5% ß-mercaptoethanol (Sigma Aldrich, M6250) protein samples were boiled and separated on precast 4-20% Criterion TGX Stain-free gels (Bio-Rad) and transferred to a nitrocellulose membrane (Amersham Protran 0.2 µm NC, #10600001). Membranes were blocked with 3% BSA in 1X Tris-buffered saline (TBS) (50mM Tris/Cl pH 7.4, 150mM NaCl) for 1 hour at room temperature. Membranes were subsequently immunoblotted overnight in primary antibody (anti-Ykt6: 1:100; anti-GAPDH: 1:500; anti-PSD95: 1:1000; anti-GluA1: 1:1000) at 4°C, shaking. The following day, membranes were washed three times with 1X TBST (TBS with 0.1% Tween) for 5 minutes and incubated in secondary IRDye antibody at 1:15000 dilution for 1 hour shaking at room temperature. Membranes were washed three times with 1X TBST for before imaging using Li-Cor Odyssey® CLx Imaging System. Images were processed and quantified using Image Studio Software (LI-COR Biosciences).

Electrophysiology

Mini EPSCs were recorded from infected primary hippocampal cultures in whole-cell voltage clamp. Recordings were performed between DIV 18-21. The external solution contained the following (in mM): 150 NaCl, 2.8 KCl, 2 $CaCl_2$, 1 $MgCl_2$, 10 glucose, and 10 m HEPES (pH adjusted to 7.3 with NaOH), with D-AP5 (50 µM), picrotoxin (50 µM), and tetrodotoxin (1µM) added. The internal solution used in recordings (in mM): 110 CsF, 30 CsCl, 10 Cs-HEPES, 5 EGTA, 4 m NaCl, and 0.5 $CaCl_2$ (pH adjusted to 7.3 with CsOH). Cells were held at −70 mV in voltage clamp with an Axopatch 200B amplifier (Molecular Devices). Data were analyzed with Clampfit version 11.0.3 (Molecular Devices).

Electron Microscopy

Samples were prepared from an adapted protocol by Arai and Waguri (153). 10 minutes at room temperature and 50 minutes at 4°C. Cells were washed with 0.12 M phosphate buffer pH 7.4 and then treated with 1% osmium tetroxide and 1.5% potassium ferrocyanide (Sigma) in 0.12M phosphate buffer pH 7.4. Cells were dehydrated by an ascending series of alcohol (50, 70, 80, 90, and 100%) followed by treatment with epoxy resin for 24 hours. The grids were mounted on resin blocks and cured at 65°C for 3 days. The blocks were trimmed to contain CSMN before proceeding to ultra-thin sectioning. Resin blocks were sectioned on a Leica Ultracut UC6 ultramicrotome (Leica Inc., Nussloch, Germany). Sections (70nm) were collected on 200 mesh copper-palladium grids. Ultra-thin sections were counterstained on a drop of UranyLess solution (Electron Microscopy Sciences, Hatfield, PA) and 0.2% lead citrate. Grids were examined on FEI Tecnai Spirit G2 TEM

(FEI Company, Hillsboro, OR) and digital images were captured on an FEI Eagle camera. Post-image acquisition adjustment was performed by Adobe Photoshop 2025.

Circular structures that were between 35 to 45 nm were considered as synaptic vesicles (77) and were manually counted. Those that were touching the membrane were counted as readily releasable pool (RRP), those close to the membrane but not touching were counted as recycling pool, and those distal to the membrane and the synaptic contact points were considered to be the reserve pool. Vesicular size was manually quantified using ImageJ.

Statistical Analysis

Graphpad Prism 10 (http://graphpad.com) was used to graph, organize, and perform all statistical analysis. Statistical analysis was determined using the following methods: in case of more than two conditions, Bartlett's Test was performed to test for homogeneity of variances. If the variances were heterogeneous, one-way analysis of variance (ANOVA) with Welch's correction alongside with Dunnett's T3 multiple comparisons test was performed; otherwise, standard ANOVA with multiple comparison was applied. In cases where two conditions were compared, F-test was performed to compare variances. If the variances were homogeneous, standard T-test was applied; otherwise, T-test with Welch's correction was used to examine the significance of the results.

For the cumulative probability distribution, the event values were binned to construct the cumulative probability, and Kormagorov-Smirnov test was applied to examine whether the distribution differed significantly from each other.

Data availability statement

All data are contained within the manuscript.

Acknowledgements

We thank Geoff Swanson for kindly allowing us to use his electrophysiology rig, Farida Korobova from the Nikon Microscopy Center for her assistance with electron microscopy, and Anis Contractor and Adrian Contreras for their critical reviews.

Funding and additional information

This study was funded by R01 NS117750 from the National Institute of Neurodegenerative Diseases and Stroke. The content is solely the responsibility of the authors and does not necessarily represent the official views of the National Institutes of Health.

Conflict of Interest

The authors declare that they have no conflicts of interest with the contents of this article.

References

1. McGrath, K., Agarwal, S., Tonelli, M., Dergai, M., Gaeta, A. L., Shum, A. K., Lacoste, J., Zhang, Y., Wen, W., Chung, D., Wiersum, G., Shevade, A., Zaichick, S., van Rossum, D. B., Shuvalova, L., Savas, J. N., Kuchin, S., Taipale, M., Caldwell, K. A., Caldwell, G. A., Fasshauer, D., and Caraveo, G. (2021) A

conformational switch driven by phosphorylation regulates the activity of the evolutionarily conserved SNARE Ykt6. Proc Natl Acad Sci U S A. 118, e2016730118
2. Malsam, J., and Söllner, T. H. (2011) Organization of SNAREs within the Golgi Stack. Cold Spring Harb Perspect Biol. 3, a005249
3. Ji, J., Yu, Y., Wu, S., Wang, D., Weng, J., and Wang, W. (2023) Different conformational dynamics of SNARE protein Ykt6 among yeast and mammals. Journal of Biological Chemistry. 10.1016/j.jbc.2023.104968
4. Cuddy, L. K., Wani, W. Y., Morella, M. L., Pitcairn, C., Tsutsumi, K., Fredriksen, K., Justman, C. J., Grammatopoulos, T. N., Belur, N. R., Zunke, F., Subramanian, A., Affaneh, A., Lansbury, P. T., and Mazzulli, J. R. (2019) Stress-Induced Cellular Clearance Is Mediated by the SNARE Protein ykt6 and Disrupted by α-Synuclein. Neuron. 104, 869-884.e11
5. Pitcairn, C., Murata, N., Zalon, A., Stojkovska, I., and Mazzulli, J. R. (2023) Impaired autophagic-lysosomal fusion in Parkinson's patient midbrain neurons occurs through loss of ykt6 and is rescued by farnesyltransferase inhibition. J Neurosci. 10.1523/jneurosci.0610-22.2023
6. Matsui, T., Jiang, P., Nakano, S., Sakamaki, Y., Yamamoto, H., and Mizushima, N. (2018) Autophagosomal YKT6 is required for fusion with lysosomes independently of syntaxin 17. Journal of Cell Biology. 217, 2633–2645
7. Gao, J., Reggiori, F., and Ungermann, C. (2018) A novel in vitro assay reveals SNARE topology and the role of Ykt6 in autophagosome fusion with vacuoles. J Cell Biol. 217, 3670–3682
8. Gao, J., Kurre, R., Rose, J., Walter, S., Fröhlich, F., Piehler, J., Reggiori, F., and Ungermann, C. (2020) Function of the SNARE Ykt6 on autophagosomes requires the Dsl1 complex and the Atg1 kinase complex. EMBO reports. 21, e50733
9. Takáts, S., Glatz, G., Szenci, G., Boda, A., Horváth, G. V., Hegedűs, K., Kovács, A. L., and Juhász, G. (2018) Non-canonical role of the SNARE protein Ykt6 in autophagosome-lysosome fusion. PLoS Genet. 14, e1007359
10. Kriegenburg, F., Bas, L., Gao, J., Ungermann, C., and Kraft, C. (2019) The multi-functional SNARE protein Ykt6 in autophagosomal fusion processes. Cell Cycle. 18, 639–651
11. Wen, W., Yu, J., Pan, L., Wei, Z., Weng, J., Wang, W., Ong, Y. S., Tran, T. H. T., Hong, W., and Zhang, M. (2010) Lipid-Induced conformational switch controls fusion activity of longin domain SNARE Ykt6. Mol Cell. 37, 383–395
12. Weng, J., Yang, Y., and Wang, W. (2015) Lipid regulated conformational dynamics of the longin SNARE protein Ykt6 revealed by molecular dynamics simulations. J Phys Chem A. 119, 1554–1562
13. Karuna M, P., Witte, L., Linnemannstoens, K., Choezom, D., Danieli-Mackay, A., Honemann-Capito, M., and Gross, J. C. (2020) Phosphorylation of Ykt6 SNARE Domain Regulates Its Membrane Recruitment and Activity. Biomolecules. 10, 1560
14. McNew, J. A., Søgaard, M., Lampen, N. M., Machida, S., Ye, R. R., Lacomis, L., Tempst, P., Rothman, J. E., and Söllner, T. H. (1997) Ykt6p, a Prenylated SNARE Essential for Endoplasmic Reticulum-Golgi Transport*. Journal of Biological Chemistry. 272, 17776–17783
15. Shirakawa, R., Goto‐Ito, S., Goto, K., Wakayama, S., Kubo, H., Sakata, N., Trinh, D. A., Yamagata, A., Sato, Y., Masumoto, H., Cheng, J., Fujimoto, T., Fukai, S., and Horiuchi, H. (2020) A SNARE geranylgeranyltransferase essential for the organization of the Golgi apparatus. EMBO J. 10.15252/embj.2019104120
16. Meiringer, C. T. A., Auffarth, K., Hou, H., and Ungermann, C. (2008) Depalmitoylation of Ykt6 Prevents its Entry into the Multivesicular Body Pathway. Traffic. 9, 1510–1521
17. Tsunemi, T., Ishiguro, Y., Yoroisaka, A., Feng, D., Shimada, T., Niiyama, S., Sasazawa, Y., Ishikawa, K., Akamatsu, W., and Hattori, N. (2025) Alpha-synuclein inhibits the secretion of extracellular vesicles through disruptions in YKT6 lipidation. J. Neurosci. 10.1523/JNEUROSCI.2350-23.2024
18. Dai, Y., Seeger, M., Weng, J., Song, S., Wang, W., and Tan, Y.-W. (2016) Lipid Regulated Intramolecular Conformational Dynamics of SNARE-Protein Ykt6. Sci Rep. 6, 30282
19. Dietrich, L. E., Gurezka, R., Veit, M., and Ungermann, C. (2004) The SNARE Ykt6 mediates protein palmitoylation during an early stage of homotypic vacuole fusion. The EMBO Journal. 23, 45–53
20. Huganir, R. L., and Nicoll, R. A. (2013) AMPARs and Synaptic Plasticity: The Last 25 Years. Neuron. 80, 704–717
21. Stockwell, I., Watson, J. F., and Greger, I. H. (2024) Tuning synaptic strength by regulation of AMPA glutamate receptor localization. BioEssays. 46, 2400006

22. Diering, G. H., and Huganir, R. L. (2018) The AMPA Receptor Code of Synaptic Plasticity. Neuron. 100, 314–329
23. Wu, Q.-L., Gao, Y., Li, J.-T., Ma, W.-Y., and Chen, N.-H. (2022) The Role of AMPARs Composition and Trafficking in Synaptic Plasticity and Diseases. Cell Mol Neurobiol. 42, 2489–2504
24. Makino, H., and Malinow, R. (2009) AMPA receptor incorporation into synapses during LTP: the role of lateral movement and exocytosis. Neuron. 64, 381–390
25. Bonnet, C., Charpentier, J., Retailleau, N., Choquet, D., and Coussen, F. Regulation of different phases of AMPA receptor intracellular transport by 4.1N and SAP97. eLife. 12, e85609
26. Hausser, A., and Schlett, K. (2019) Coordination of AMPA receptor trafficking by Rab GTPases. Small GTPases. 10, 419–432
27. Wamsley, J. K. (1992) Transport of receptors. Mol Neurobiol. 6, 313–321
28. Valenzuela, J. I., and Perez, F. (2015) Diversifying the secretory routes in neurons. Front Neurosci. 9, 358
29. Esteves da Silva, M., Adrian, M., Schätzle, P., Lipka, J., Watanabe, T., Cho, S., Futai, K., Wierenga, C. J., Kapitein, L. C., and Hoogenraad, C. C. (2015) Positioning of AMPA Receptor-Containing Endosomes Regulates Synapse Architecture. Cell Reports. 13, 933–943
30. Yang, Y., Wang, X., Frerking, M., and Zhou, Q. (2008) Delivery of AMPA receptors to perisynaptic sites precedes the full expression of long-term potentiation. Proceedings of the National Academy of Sciences. 105, 11388–11393
31. Schwenk, J., and Fakler, B. (2021) Building of AMPA-type glutamate receptors in the endoplasmic reticulum and its implication for excitatory neurotransmission. The Journal of Physiology. 599, 2639–2653
32. Brechet, A., Buchert, R., Schwenk, J., Boudkkazi, S., Zolles, G., Siquier-Pernet, K., Schaber, I., Bildl, W., Saadi, A., Bole-Feysot, C., Nitschke, P., Reis, A., Sticht, H., Al-Sanna'a, N., Rolfs, A., Kulik, A., Schulte, U., Colleaux, L., Abou Jamra, R., and Fakler, B. (2017) AMPA-receptor specific biogenesis complexes control synaptic transmission and intellectual ability. Nat Commun. 8, 15910
33. Shi, S.-H., Hayashi, Y., Esteban, J. A., and Malinow, R. (2001) Subunit-specific rules governing AMPA receptor trafficking to synapses in hippocampal pyramidal neurons. Cell. 105, 331–343
34. Lu, W., Shi, Y., Jackson, A. C., Bjorgan, K., During, M. J., Sprengel, R., Seeburg, P. H., and Nicoll, R. A. (2009) Subunit composition of synaptic AMPA receptors revealed by a single-cell genetic approach. Neuron. 62, 254–268
35. Perestenko, P. V., and Henley, J. M. (2003) Characterization of the intracellular transport of GluR1 and GluR2 alpha-amino-3-hydroxy-5-methyl-4-isoxazole propionic acid receptor subunits in hippocampal neurons. J Biol Chem. 278, 43525–43532
36. Lu, W., Isozaki, K., Roche, K. W., and Nicoll, R. A. (2010) Synaptic targeting of AMPA receptors is regulated by a CaMKII site in the first intracellular loop of GluA1. Proceedings of the National Academy of Sciences. 107, 22266–22271
37. Middei, S., Ammassari-Teule, M., and Marie, H. (2014) Synaptic plasticity under learning challenge. Neurobiol Learn Mem. 115, 108–115
38. Qu, W., Yuan, B., Liu, J., Liu, Q., Zhang, X., Cui, R., Yang, W., and Li, B. (2021) Emerging role of AMPA receptor subunit GluA1 in synaptic plasticity: Implications for Alzheimer's disease. Cell Proliferation. 54, e12959
39. Mack, V., Burnashev, N., Kaiser, K. M., Rozov, A., Jensen, V., Hvalby, O., Seeburg, P. H., Sakmann, B., and Sprengel, R. (2001) Conditional restoration of hippocampal synaptic potentiation in Glur-A-deficient mice. Science. 292, 2501–2504
40. Yang, X., Gong, R., Qin, L., Bao, Y., Fu, Y., Gao, S., Yang, H., Ni, J., Yuan, T.-F., and Lu, W. (2022) Trafficking of NMDA receptors is essential for hippocampal synaptic plasticity and memory consolidation. Cell Reports. 10.1016/j.celrep.2022.111217
41. Sumi, T., and Harada, K. (2020) Mechanism underlying hippocampal long-term potentiation and depression based on competition between endocytosis and exocytosis of AMPA receptors. Sci Rep. 10, 14711
42. Kullmann, D. M., Erdemli, G., and Asztély, F. (1996) LTP of AMPA and NMDA receptor-mediated signals: evidence for presynaptic expression and extrasynaptic glutamate spill-over. Neuron. 17, 461–474
43. Lin, D.-T., Makino, Y., Sharma, K., Hayashi, T., Neve, R., Takamiya, K., and Huganir, R. L. (2009) Regulation of AMPA receptor extrasynaptic insertion by 4.1N, phosphorylation and palmitoylation. Nat Neurosci. 12, 879–887
44. Jensen, V., Kaiser, K. M. M., Borchardt, T., Adelmann, G., Rozov, A., Burnashev, N., Brix, C., Frotscher, M., Andersen, P., Hvalby, Ø., Sakmann, B., Seeburg, P. H., and Sprengel, R. (2003) A juvenile form of

postsynaptic hippocampal long-term potentiation in mice deficient for the AMPA receptor subunit GluR-A. J Physiol. 553, 843–856
45. Zamanillo, D., Sprengel, R., Hvalby, Ø., Jensen, V., Burnashev, N., Rozov, A., Kaiser, K. M. M., Köster, H. J., Borchardt, T., Worley, P., Lübke, J., Frotscher, M., Kelly, P. H., Sommer, B., Andersen, P., Seeburg, P. H., and Sakmann, B. (1999) Importance of AMPA Receptors for Hippocampal Synaptic Plasticity But Not for Spatial Learning. Science. 284, 1805–1811
46. Boehm, J., Kang, M.-G., Johnson, R. C., Esteban, J., Huganir, R. L., and Malinow, R. (2006) Synaptic incorporation of AMPA receptors during LTP is controlled by a PKC phosphorylation site on GluR1. Neuron. 51, 213–225
47. Diógenes, M. J., Dias, R. B., Rombo, D. M., Miranda, H. V., Maiolino, F., Guerreiro, P., Nässtrom, T., Franquelim, H. G., Oliveira, L. M. A., Castanho, M. A. R. B., Lannfelt, L., Bergström, J., Ingelsson, M., Quintas, A., Sebastião, A. M., Lopes, L. V., and Outeiro, T. F. (2012) Extracellular Alpha-Synuclein Oligomers Modulate Synaptic Transmission and Impair LTP Via NMDA-Receptor Activation. J. Neurosci. 32, 11750–11762
48. Iemolo, A., De Risi, M., Giordano, N., Torromino, G., Somma, C., Cavezza, D., Colucci, M., Mancini, M., de Iure, A., Granata, R., Picconi, B., Calabresi, P., and De Leonibus, E. (2023) Synaptic mechanisms underlying onset and progression of memory deficits caused by hippocampal and midbrain synucleinopathy. npj Parkinsons Dis. 9, 1–15
49. Kulkarni, A. S., Burns, M. R., Brundin, P., and Wesson, D. W. (2022) Linking α-synuclein-induced synaptopathy and neural network dysfunction in early Parkinson's disease. Brain Communications. 4, fcac165
50. Allen Institute for Brain Science (2004) Allen Brain Cell Atlas - brain-map.org. [online] https://portal.brain-map.org/atlases-and-data/bkp/abc-atlas (Accessed October 30, 2023)
51. Shen, E. H., Overly, C. C., and Jones, A. R. (2012) The Allen Human Brain Atlas: Comprehensive gene expression mapping of the human brain. Trends in Neurosciences. 35, 711–714
52. Adamowicz, D. H., Roy, S., Salmon, D. P., Galasko, D. R., Hansen, L. A., Masliah, E., and Gage, F. H. (2017) Hippocampal α-Synuclein in Dementia with Lewy Bodies Contributes to Memory Impairment and Is Consistent with Spread of Pathology. J Neurosci. 37, 1675–1684
53. Kasongo, D. W., de Leo, G., Vicario, N., Leanza, G., and Legname, G. (2020) Chronic α-Synuclein Accumulation in Rat Hippocampus Induces Lewy Bodies Formation and Specific Cognitive Impairments. eNeuro. 7, ENEURO.0009-20.2020
54. Koss, D. J., Erskine, D., Porter, A., Palmoski, P., Menon, H., Todd, O. G. J., Leite, M., Attems, J., and Outeiro, T. F. (2022) Nuclear alpha-synuclein is present in the human brain and is modified in dementia with Lewy bodies. Acta Neuropathologica Communications. 10, 98
55. Teil, M., Dovero, S., Bourdenx, M., Arotcarena, M.-L., Darricau, M., Porras, G., Thiolat, M.-L., Trigo-Damas, I., Perier, C., Estrada, C., Garcia-Carrillo, N., Herrero, M. T., Vila, M., Obeso, J. A., Bezard, E., and Dehay, B. (2023) Cortical Lewy body injections induce long-distance pathogenic alterations in the non-human primate brain. npj Parkinsons Dis. 9, 1–13
56. Wirdefeldt, K., Bogdanovic, N., Westerberg, L., Payami, H., Schalling, M., and Murdoch, G. (2001) Expression of α-synuclein in the human brain: relation to Lewy body disease. Molecular Brain Research. 92, 58–65
57. Altay, M. F., Liu, A. K. L., Holton, J. L., Parkkinen, L., and Lashuel, H. A. (2022) Prominent astrocytic alpha-synuclein pathology with unique post-translational modification signatures unveiled across Lewy body disorders. Acta Neuropathologica Communications. 10, 163
58. Dues, D. J., Nguyen, A. P. T., Becker, K., Ma, J., and Moore, D. J. (2023) Hippocampal subfield vulnerability to α-synuclein pathology precedes neurodegeneration and cognitive dysfunction. npj Parkinsons Dis. 9, 1–11
59. Hashimoto, M., and Masliah, E. (2006) Alpha‐synuclein in Lewy Body Disease and Alzheimer's Disease. Brain Pathol. 9, 707–720
60. Marotta, N. P., Ara, J., Uemura, N., Lougee, M. G., Meymand, E. S., Zhang, B., Petersson, E. J., Trojanowski, J. Q., and Lee, V. M.-Y. (2021) Alpha-synuclein from patient Lewy bodies exhibits distinct pathological activity that can be propagated in vitro. Acta Neuropathologica Communications. 9, 188
61. Sanderson, J. B., De, S., Jiang, H., Rovere, M., Jin, M., Zaccagnini, L., Hays Watson, A., De Boni, L., Lagomarsino, V. N., Young-Pearse, T. L., Liu, X., Pochapsky, T. C., Hyman, B. T., Dickson, D. W., Klenerman, D., Selkoe, D. J., and Bartels, T. (2020) Analysis of α-synuclein species enriched from cerebral cortex of humans with sporadic dementia with Lewy bodies. Brain Communications. 2, fcaa010

62. Lippa, C. F., Fujiwara, H., Mann, D. M. A., Giasson, B., Baba, M., Schmidt, M. L., Nee, L. E., O'Connell, B., Pollen, D. A., St. George-Hyslop, P., Ghetti, B., Nochlin, D., Bird, T. D., Cairns, N. J., Lee, V. M.-Y., Iwatsubo, T., and Trojanowski, J. Q. (1998) Lewy Bodies Contain Altered α-Synuclein in Brains of Many Familial Alzheimer's Disease Patients with Mutations in Presenilin and Amyloid Precursor Protein Genes. The American Journal of Pathology. 153, 1365–1370
63. Lippa, C. F., Duda, J. E., Grossman, M., Hurtig, H. I., Aarsland, D., Boeve, B. F., Brooks, D. J., Dickson, D. W., Dubois, B., Emre, M., Fahn, S., Farmer, J. M., Galasko, D., Galvin, J. E., Goetz, C. G., Growdon, J. H., Gwinn-Hardy, K. A., Hardy, J., Heutink, P., Iwatsubo, T., Kosaka, K., Lee, V. M.-Y., Leverenz, J. B., Masliah, E., McKeith, I. G., Nussbaum, R. L., Olanow, C. W., Ravina, B. M., Singleton, A. B., Tanner, C. M., Trojanowski, J. Q., and Wszolek, Z. K. (2007) DLB and PDD boundary issues: Diagnosis, treatment, molecular pathology, and biomarkers. Neurology. 68, 812–819
64. Colom-Cadena, M., Pegueroles, J., Herrmann, A. G., Henstridge, C. M., Muñoz, L., Querol-Vilaseca, M., Martín-Paniello, C. S., Luque-Cabecerans, J., Clarimon, J., Belbin, O., Núñez-Llaves, R., Blesa, R., Smith, C., McKenzie, C.-A., Frosch, M. P., Roe, A., Fortea, J., Andilla, J., Loza-Alvarez, P., Gelpi, E., Hyman, B. T., Spires-Jones, T. L., and Lleó, A. (2017) Synaptic phosphorylated α-synuclein in dementia with Lewy bodies. Brain. 140, 3204–3214
65. Zhang, T., and Hong, W. (2001) Ykt6 Forms a SNARE Complex with Syntaxin 5, GS28, and Bet1 and Participates in a Late Stage in Endoplasmic Reticulum-Golgi Transport*. Journal of Biological Chemistry. 276, 27480–27487
66. Stewart, M. G., Medvedev, N. I., Popov, V. I., Schoepfer, R., Davies, H. A., Murphy, K., Dallérac, G. M., Kraev, I. V., and Rodríguez, J. J. (2005) Chemically induced long-term potentiation increases the number of perforated and complex postsynaptic densities but does not alter dendritic spine volume in CA1 of adult mouse hippocampal slices. Eur J Neurosci. 21, 3368–3378
67. Fortin, D. A., Davare, M. A., Srivastava, T., Brady, J. D., Nygaard, S., Derkach, V. A., and Soderling, T. R. (2010) Long-Term Potentiation-Dependent Spine Enlargement Requires Synaptic Ca2+-Permeable AMPA Receptors Recruited by CaM-Kinase I. J Neurosci. 30, 11565–11575
68. Divakaruni, S. S., Van Dyke, A. M., Chandra, R., LeGates, T. A., Contreras, M., Dharmasri, P. A., Higgs, H. N., Lobo, M. K., Thompson, S. M., and Blanpied, T. A. (2018) Long-Term Potentiation Requires a Rapid Burst of Dendritic Mitochondrial Fission during Induction. Neuron. 100, 860-875.e7
69. Fujii, S., Sasaki, H., Mikoshiba, K., Kuroda, Y., Yamazaki, Y., Mostafa Taufiq, A., and Kato, H. (2004) A chemical LTP induced by co-activation of metabotropic and N-methyl-d-aspartate glutamate receptors in hippocampal CA1 neurons. Brain Research. 999, 20–28
70. Jin, C., Jang, S.-S., Ge, P., Chung, H. J., and Selvin, P. (2021) Single molecule tracking of AMPA receptors shows the role of synaptic insertion during maintenance of chemical LTP. 10.1101/2021.02.04.429665
71. Lu, W.-Y., Man, H.-Y., Ju, W., Trimble, W. S., MacDonald, J. F., and Wang, Y. T. (2001) Activation of Synaptic NMDA Receptors Induces Membrane Insertion of New AMPA Receptors and LTP in Cultured Hippocampal Neurons. Neuron. 29, 243–254
72. Chiu, A. M., Barse, L., Hubalkova, P., and Sanz-Clemente, A. (2019) An Antibody Feeding Approach to Study Glutamate Receptor Trafficking in Dissociated Primary Hippocampal Cultures. J Vis Exp. 10.3791/59982
73. Penn, A. C., Williams, S. R., and Greger, I. H. (2008) Gating motions underlie AMPA receptor secretion from the endoplasmic reticulum. The EMBO Journal. 27, 3056–3068
74. Morise, J., Suzuki, K. G. N., Kitagawa, A., Wakazono, Y., Takamiya, K., Tsunoyama, T. A., Nemoto, Y. L., Takematsu, H., Kusumi, A., and Oka, S. (2019) AMPA receptors in the synapse turnover by monomer diffusion. Nat Commun. 10, 5245
75. Lüscher, C., Xia, H., Beattie, E. C., Carroll, R. C., von Zastrow, M., Malenka, R. C., and Nicoll, R. A. (1999) Role of AMPA receptor cycling in synaptic transmission and plasticity. Neuron. 24, 649–658
76. Rizzoli, S. O., and Betz, W. J. (2005) Synaptic vesicle pools. Nat Rev Neurosci. 6, 57–69
77. Südhof, T. C. (1999) Composition of Synaptic Vesicles. in Basic Neurochemistry: Molecular, Cellular and Medical Aspects. 6th edition, Lippincott-Raven, [online] https://www.ncbi.nlm.nih.gov/books/NBK28154/ (Accessed February 8, 2025)
78. Peng, Y.-R., He, S., Marie, H., Zeng, S.-Y., Ma, J., Tan, Z.-J., Lee, S. Y., Malenka, R. C., and Yu, X. (2009) Coordinated changes in dendritic arborization and synaptic strength during neural circuit development. Neuron. 61, 71–84

79. Kirchner, J. H., Euler, L., Fritz, I., Castro, A. F., and Gjorgjieva, J. (2024) Dendritic growth and synaptic organization from activity-independent cues and local activity-dependent plasticity. eLife. 10.7554/eLife.87527.2
80. Wen, Q., Stepanyants, A., Elston, G. N., Grosberg, A. Y., and Chklovskii, D. B. (2009) Maximization of the connectivity repertoire as a statistical principle governing the shapes of dendritic arbors. Proceedings of the National Academy of Sciences. 106, 12536–12541
81. Jan, Y.-N., and Jan, L. Y. (2010) Branching out: mechanisms of dendritic arborization. Nat Rev Neurosci. 11, 316–328
82. Meltzer, S., Bagley, J. A., Perez, G. L., O'Brien, C. E., DeVault, L., Guo, Y., Jan, L. Y., and Jan, Y.-N. (2017) Phospholipid homeostasis regulates dendrite morphogenesis in Drosophila sensory neurons. Cell Rep. 21, 859–866
83. Chen, M., Xu, L., Wu, Y., Soba, P., and Hu, C. (2023) The organization and function of the Golgi apparatus in dendrite development and neurological disorders. Genes & Diseases. 10, 2425–2442
84. Schneider, C. A., Rasband, W. S., and Eliceiri, K. W. (2012) NIH Image to ImageJ: 25 years of image analysis. Nat Methods. 9, 671–675
85. Hage, T. A., Sun, Y., and Khaliq, Z. M. (2016) Electrical and Ca2+ signaling in dendritic spines of substantia nigra dopaminergic neurons. eLife. 5, e13905
86. Ratliff, W. A., Delic, V., Pick, C. G., and Citron, B. A. (2020) Dendritic arbor complexity and spine density changes after repetitive mild traumatic brain injury and neuroprotective treatments. Brain Res. 1746, 147019
87. Hsieh, H., Boehm, J., Sato, C., Iwatsubo, T., Tomita, T., Sisodia, S., and Malinow, R. (2006) AMPA-R Removal Underlies Aβ-induced Synaptic Depression and Dendritic Spine Loss. Neuron. 52, 831–843
88. Turrigiano, G. G., and Nelson, S. B. (2004) Homeostatic plasticity in the developing nervous system. Nat Rev Neurosci. 5, 97–107
89. Tian, X., Teng, J., and Chen, J. (2021) New insights regarding SNARE proteins in autophagosome-lysosome fusion. Autophagy. 17, 2680–2688
90. Sakata, N., Shirakawa, R., Goto, K., Trinh, D. A., and Horiuchi, H. (2021) Double prenylation of SNARE protein Ykt6 is required for lysosomal hydrolase trafficking. The Journal of Biochemistry. 169, 363–370
91. Yong, C. Q. Y., and Tang, B. L. (2019) Another longin SNARE for autophagosome-lysosome fusion-how does Ykt6 work? Autophagy. 15, 352–357
92. Lee, C., Lepore, D., Lee, S.-H., Kim, T. G., Buwa, N., Lee, J., Munson, M., and Yoon, T.-Y. (2024) Exocyst stimulates multiple steps of exocytic SNARE complex assembly and vesicle fusion. Nat Struct Mol Biol. 10.1038/s41594-024-01388-2
93. Hasegawa, H., Zinsser, S., Rhee, Y., Vik-Mo, E. O., Davanger, S., and Hay, J. C. (2003) Mammalian Ykt6 Is a Neuronal SNARE Targeted to a Specialized Compartment by its Profilin-like Amino Terminal Domain. MBoC. 14, 698–720
94. Watanabe, H., Urano, S., Kikuchi, N., Kubo, Y., Kikuchi, A., Gomi, K., and Shintani, T. (2024) Ykt6 functionally overlaps with vacuolar and exocytic R-SNAREs in the yeast Saccharomyces cerevisiae. Journal of Biological Chemistry. 10.1016/j.jbc.2024.107274
95. Pokrywka, N. J., Bush, S., and Nick, S. E. (2022) The R-SNARE Ykt6 is required for multiple events during oogenesis in Drosophila. Cells & Development. 169, 203759
96. Overhoff, M., Tellkamp, F., Hess, S., Tutas, J., Tolve, M., Faerfers, M., Ickert, L., Mohammadi, M., Bruyckere, E. D., Kallergi, E., Vedove, A. D., Nikoletopoulou, V., Wirth, B., Isensee, J., Hucho, T., Puchkov, D., Isbrandt, D., Krüger, M., Kloppenburg, P., and Kononenko, N. L. (2022) Autophagy regulates neuronal excitability by controlling cAMP/Protein Kinase A signaling. 10.1101/2022.02.11.480034
97. Shehata, M., Abdou, K., Choko, K., Matsuo, M., Nishizono, H., and Inokuchi, K. (2018) Autophagy Enhances Memory Erasure through Synaptic Destabilization. J. Neurosci. 38, 3809–3822
98. Shehata, M., Matsumura, H., Okubo-Suzuki, R., Ohkawa, N., and Inokuchi, K. (2012) Neuronal Stimulation Induces Autophagy in Hippocampal Neurons That Is Involved in AMPA Receptor Degradation after Chemical Long-Term Depression. Journal of Neuroscience. 32, 10413–10422
99. Goo, M. S., Sancho, L., Slepak, N., Boassa, D., Deerinck, T. J., Ellisman, M. H., Bloodgood, B. L., and Patrick, G. N. (2017) Activity-dependent trafficking of lysosomes in dendrites and dendritic spines. Journal of Cell Biology. 216, 2499–2513
100. Hanley, J. G. (2018) The Regulation of AMPA Receptor Endocytosis by Dynamic Protein-Protein Interactions. Front. Cell. Neurosci. 10.3389/fncel.2018.00362

101. Lin, J. W., Ju, W., Foster, K., Lee, S. H., Ahmadian, G., Wyszynski, M., Wang, Y. T., and Sheng, M. (2000) Distinct molecular mechanisms and divergent endocytotic pathways of AMPA receptor internalization. Nature Neuroscience. 3, 1282–1290
102. Liu, W., Gao, T., Li, N., Shao, S., and Liu, B. (2024) Vesicle fusion and release in neurons under dynamic mechanical equilibrium. iScience. 27, 109793
103. Hong, W. (2005) SNAREs and traffic. Biochimica et Biophysica Acta (BBA) - Molecular Cell Research. 1744, 120–144
104. Jurado, S. (2014) The dendritic SNARE fusion machinery involved in AMPARs insertion during long-term potentiation. Front. Cell. Neurosci. 10.3389/fncel.2014.00407
105. Kuster, A., Nola, S., Dingli, F., Vacca, B., Gauchy, C., Beaujouan, J.-C., Nunez, M., Moncion, T., Loew, D., Formstecher, E., Galli, T., and Proux-Gillardeaux, V. (2015) The Q-soluble N-Ethylmaleimide-sensitive Factor Attachment Protein Receptor (Q-SNARE) SNAP-47 Regulates Trafficking of Selected Vesicle-associated Membrane Proteins (VAMPs). J Biol Chem. 290, 28056–28069
106. Urbina, F. L., Menon, S., Goldfarb, D., Edwards, R., Ben Major, M., Brennwald, P., and Gupton, S. L. (2021) TRIM67 regulates exocytic mode and neuronal morphogenesis via SNAP47. Cell Reports. 34, 108743
107. Holt, M., Varoqueaux, F., Wiederhold, K., Takamori, S., Urlaub, H., Fasshauer, D., and Jahn, R. (2006) Identification of SNAP-47, a Novel Qbc-SNARE with Ubiquitous Expression *. Journal of Biological Chemistry. 281, 17076–17083
108. Yan, C., Jiang, J., Yang, Y., Geng, X., and Dong, W. (2022) The function of VAMP2 in mediating membrane fusion: An overview. Front. Mol. Neurosci. 10.3389/fnmol.2022.948160
109. Alvarez-Castelao, B., and Schuman, E. M. (2015) The Regulation of Synaptic Protein Turnover. J Biol Chem. 290, 28623–28630
110. Steward, O., and Schuman, E. M. (2003) Compartmentalized synthesis and degradation of proteins in neurons. Neuron. 40, 347–359
111. Bollmann, C., Schöning, S., Kotschnew, K., Grosse, J., Heitzig, N., and Fischer von Mollard, G. (2022) Primary neurons lacking the SNAREs vti1a and vti1b show altered neuronal development. Neural Dev. 17, 12
112. Kemal, S., Richardson, H. S., Dyne, E. D., and Fu, M. (2022) ER and Golgi trafficking in axons, dendrites, and glial processes. Current Opinion in Cell Biology. 78, 102119
113. Evans, A. J., Gurung, S., Wilkinson, K. A., Stephens, D. J., and Henley, J. M. (2017) Assembly, Secretory Pathway Trafficking, and Surface Delivery of Kainate Receptors Is Regulated by Neuronal Activity. Cell Reports. 19, 2613–2626
114. Hanus, C., and Ehlers, M. D. (2008) Secretory outposts for the local processing of membrane cargo in neuronal dendrites. Traffic. 9, 1437–1445
115. Horton, A. C., Rácz, B., Monson, E. E., Lin, A. L., Weinberg, R. J., and Ehlers, M. D. (2005) Polarized Secretory Trafficking Directs Cargo for Asymmetric Dendrite Growth and Morphogenesis. Neuron. 48, 757–771
116. Bowen, A. B., Bourke, A. M., Hiester, B. G., Hanus, C., and Kennedy, M. J. (2017) Golgi-independent secretory trafficking through recycling endosomes in neuronal dendrites and spines. eLife. 6, e27362
117. Aridor, M., Guzik, A. K., Bielli, A., and Fish, K. N. (2004) Endoplasmic Reticulum Export Site Formation and Function in Dendrites. J Neurosci. 24, 3770–3776
118. Pick, J. E., and Ziff, E. B. (2018) Regulation of AMPA Receptor Trafficking and Exit from the Endoplasmic Reticulum. Mol Cell Neurosci. 91, 3–9
119. Grochowska, K. M., Andres-Alonso, M., Karpova, A., and Kreutz, M. R. (2022) The needs of a synapse—How local organelles serve synaptic proteostasis. The EMBO Journal. 10.15252/embj.2021110057
120. O'Sullivan, M. J., and Lindsay, A. J. (2020) The Endosomal Recycling Pathway—At the Crossroads of the Cell. Int J Mol Sci. 21, 6074
121. John Jacob Peters, Leitz, J., Oses-Prieto, J. A., Burlingame, A. L., and Brunger, A. T. (2021) Molecular Characterization of AMPA-Receptor-Containing Vesicles. Frontiers in Molecular Neuroscience. 10.3389/fnmol.2021.754631
122. Henley, J. M., and Wilkinson, K. A. (2013) AMPA receptor trafficking and the mechanisms underlying synaptic plasticity and cognitive aging. Dialogues Clin Neurosci. 15, 11–27
123. Govind, A. P., Jeyifous, O., Russell, T. A., Yi, Z., Weigel, A. V., Ramaprasad, A., Newell, L., Ramos, W., Valbuena, F. M., Casler, J. C., Yan, J.-Z., Glick, B. S., Swanson, G. T., Lippincott-Schwartz, J., and Green,

W. N. (2021) Activity-dependent Golgi satellite formation in dendrites reshapes the neuronal surface glycoproteome. eLife. 10, e68910
124. Kennedy, G., Gibson, O., T. O'Hare, D., Mills, I. G., and Evergren, E. (2023) The role of CaMKK2 in Golgi-associated vesicle trafficking. Biochem Soc Trans. 51, 331–342
125. Wang, Z., Palmer, G., and Griffith, L. C. (1998) Regulation of Drosophila Ca2+/calmodulin-dependent protein kinase II by autophosphorylation analyzed by site-directed mutagenesis. J Neurochem. 71, 378–387
126. Mikhaylova, M., Hradsky, J., and Kreutz, M. R. (2011) Between promiscuity and specificity: novel roles of EF-hand calcium sensors in neuronal Ca2+ signalling. Journal of Neurochemistry. 118, 695–713
127. Hanus, C., Kochen, L., Dieck, S. tom, Racine, V., Sibarita, J.-B., Schuman, E. M., and Ehlers, M. D. (2014) Synaptic Control of Secretory Trafficking in Dendrites. Cell Rep. 7, 1771–1778
128. Alexander, G. E. (2004) Biology of Parkinson's disease: pathogenesis and pathophysiology of a multisystem neurodegenerative disorder. Dialogues Clin Neurosci. 6, 259–280
129. Armstrong, R. (1998) Lewy body and Alzheimer pathology in temporal lobe in dementia with Lewy bodies. Alzheimer's Reports. 1, 159–163
130. Chin, K. S. (2023) Pathophysiology of dementia
131. Jellinger, K. A. (2024) Behavioral disorders in dementia with Lewy bodies: old and new knowledge. J Neural Transm. 10.1007/s00702-024-02823-w
132. Jellinger, K. A., and Korczyn, A. D. (2018) Are dementia with Lewy bodies and Parkinson's disease dementia the same disease? BMC Medicine. 16, 34
133. Kingwell, K. (2017) Zeroing in on neurodegenerative α-synuclein. Nature Reviews Drug Discovery. 16, 371–373
134. Thayanidhi, N., Helm, J. R., Nycz, D. C., Bentley, M., Liang, Y., and Hay, J. C. (2010) a-Synuclein Delays Endoplasmic Reticulum (ER)-to-Golgi. Molecular Biology of the Cell
135. Caraveo, G., Soste, M., Cappelleti, V., Fanning, S., van Rossum, D. B., Whitesell, L., Huang, Y., Chung, C. Y., Baru, V., Zaichick, S., Picotti, P., and Lindquist, S. (2017) FKBP12 contributes to α-synuclein toxicity by regulating the calcineurin-dependent phosphoproteome. Proc Natl Acad Sci U S A. 114, E11313–E11322
136. Calabresi, P., Di Lazzaro, G., Marino, G., Campanelli, F., and Ghiglieri, V. (2023) Advances in understanding the function of alpha-synuclein: implications for Parkinson's disease. Brain. 146, 3587–3597
137. Ghiglieri, V., Calabrese, V., and Calabresi, P. (2018) Alpha-Synuclein: From Early Synaptic Dysfunction to Neurodegeneration. Front. Neurol. 10.3389/fneur.2018.00295
138. Sharma, M., and Burré, J. (2023) α-Synuclein in synaptic function and dysfunction. Trends in Neurosciences. 46, 153–166
139. Jurado, S. (2018) AMPA Receptor Trafficking in Natural and Pathological Aging. Front Mol Neurosci. 10, 446
140. da Silva, J. A. C., and Schröder, N. (2023) The Role of Ca2+ Permeable AMPA Receptors in Neurodegeneration, Neurotoxicity, and Neuroinflammation. CNS Neurol Disord Drug Targets. 22, 624–633
141. Wright, A. L., Konen, L. M., Mockett, B. G., Morris, G. P., Singh, A., Burbano, L. E., Milham, L., Hoang, M., Zinn, R., Chesworth, R., Tan, R. P., Royle, G. A., Clark, I., Petrou, S., Abraham, W. C., and Vissel, B. (2023) The Q/R editing site of AMPA receptor GluA2 subunit acts as an epigenetic switch regulating dendritic spines, neurodegeneration and cognitive deficits in Alzheimer's disease. Molecular Neurodegeneration. 18, 65
142. Zhang, H., and Bramham, C. R. (2020) Bidirectional Dysregulation of AMPA Receptor-Mediated Synaptic Transmission and Plasticity in Brain Disorders. Front. Synaptic Neurosci. 10.3389/fnsyn.2020.00026
143. Kwak, S., and Weiss, J. H. (2006) Calcium-permeable AMPA channels in neurodegenerative disease and ischemia. Current Opinion in Neurobiology. 16, 281–287
144. Guo, C., and Ma, Y.-Y. (2021) Calcium Permeable-AMPA Receptors and Excitotoxicity in Neurological Disorders. Front. Neural Circuits. 10.3389/fncir.2021.711564
145. Italia, M., Ferrari, E., Di Luca, M., and Gardoni, F. (2021) GluA3-containing AMPA receptors: From physiology to synaptic dysfunction in brain disorders. Neurobiology of Disease. 161, 105539
146. Feldmeyer, D., Kask, K., Brusa, R., Kornau, H.-C., Kolhekar, R., Rozov, A., Burnashev, N., Jensen, V., Hvalby, Ø., Sprengel, R., and Seeburg, P. H. (1999) Neurological dysfunctions in mice expressing different levels of the Q/R site–unedited AMPAR subunit GluR–B. Nat Neurosci. 2, 57–64

147. Hettinger, J. C., Lee, H., Bu, G., Holtzman, D. M., and Cirrito, J. R. (2018) AMPA-ergic regulation of amyloid-β levels in an Alzheimer's disease mouse model. Molecular Neurodegeneration. 13, 22
148. Lu, K., Li, C., Liu, J., Wang, J., Li, Y., He, B., Li, J., Zhang, X., Wei, M., Tian, Y., Zhang, R., Zhang, C., and Zhang, Y. (2023) Impairments in endogenous AMPA receptor dynamics correlates with learning deficits in Alzheimer's disease model mice. Proceedings of the National Academy of Sciences. 120, e2303878120
149. Bennett, M. V. L., Pellegrini-Giampietro, D. E., Gorter, J. A., Aronica, E., Connor, J. A., and Zukin, R. S. (1996) The GluR2 Hypothesis: Ca++-permeable AMPA Receptors in Delayed Neurodegeneration. Cold Spring Harb Symp Quant Biol. 61, 373–384
150. Ferreira, T. A., Blackman, A. V., Oyrer, J., Jayabal, S., Chung, A. J., Watt, A. J., Sjöström, P. J., and van Meyel, D. J. (2014) Neuronal morphometry directly from bitmap images. Nat Methods. 11, 982–984
151. McCall, A. D. (2024) Colocalization by cross-correlation, a new method of colocalization suited for super-resolution microscopy. BMC Bioinformatics. 25, 55
152. Bermejo, M. K., Milenkovic, M., Salahpour, A., and Ramsey, A. J. (2014) Preparation of Synaptic Plasma Membrane and Postsynaptic Density Proteins Using a Discontinuous Sucrose Gradient. J Vis Exp. 10.3791/51896
153. Arai, R., and Waguri, S. (2019) Improved Electron Microscopy Fixation Methods for Tracking Autophagy-Associated Membranes in Cultured Mammalian Cells. Methods Mol Biol. 1880, 211–221
154. Hawrylycz, M. J., Lein, E. S., Guillozet-Bongaarts, A. L., Shen, E. H., Ng, L., Miller, J. A., van de Lagemaat, L. N., Smith, K. A., Ebbert, A., Riley, Z. L., Abajian, C., Beckmann, C. F., Bernard, A., Bertagnolli, D., Boe, A. F., Cartagena, P. M., Chakravarty, M. M., Chapin, M., Chong, J., Dalley, R. A., David Daly, B., Dang, C., Datta, S., Dee, N., Dolbeare, T. A., Faber, V., Feng, D., Fowler, D. R., Goldy, J., Gregor, B. W., Haradon, Z., Haynor, D. R., Hohmann, J. G., Horvath, S., Howard, R. E., Jeromin, A., Jochim, J. M., Kinnunen, M., Lau, C., Lazarz, E. T., Lee, C., Lemon, T. A., Li, L., Li, Y., Morris, J. A., Overly, C. C., Parker, P. D., Parry, S. E., Reding, M., Royall, J. J., Schulkin, J., Sequeira, P. A., Slaughterbeck, C. R., Smith, S. C., Sodt, A. J., Sunkin, S. M., Swanson, B. E., Vawter, M. P., Williams, D., Wohnoutka, P., Zielke, H. R., Geschwind, D. H., Hof, P. R., Smith, S. M., Koch, C., Grant, S. G. N., and Jones, A. R. (2012) An anatomically comprehensive atlas of the adult human brain transcriptome. Nature. 489, 391–399

Figure Captions

Figure 1.

Ykt6 is highly expressed in the hippocampus in the mammalian brain. A) Top, Sagittal view of the Ykt6 expression by in-situ hybridization assay and microarray with two Ykt6 probes in healthy adult human brains. Allen Human Brain Atlas, https://human.brain-map.org/microarray/search/show?search_type=user_selections&user_selection_mode=2. Bottom panel, quantification of Ykt6 and Microtubule-associated protein 2 (MAP2) from the indicated brain regions (154). N=6 humans; MAP2 serves as a metric for high expression. Error bars represent standard deviation. **B)** Ykt6 expression by fluorescence in-situ hybridization in a sagittal section from a mouse brain. Allen Mouse Brain Atlas, https://mouse.brain-map.org/experiment/show/71380453.

Figure 2.

Ykt6 is present in the cytosol, Golgi Apparatus, and endoplasmic reticulum at somatic and dendritic locations in hippocampal pyramidal neurons. A-H) Primary hippocampal pyramidal neurons were transduced with either ShRNA against Ykt6 (Sh Ykt6) or ShRNA scrambled sequence as Control (Sh Ctrl) at DIV5, induced for Ykt6 knockdown with doxycycline starting at DIV8 and immunostained at DIV21 with GM130 (Golgi Apparatus) and Ykt6. **A)** Representative immunofluorescence images of neurons transduced with Sh Ctrl of Golgi apparatus (magenta) and Ykt6 (cyan); scale bar, 10µm. **B)** Fluorescence intensity linescans of Golgi apparatus and Ykt6 from the soma (Box 1) in (A). **C)** Representative immunofluorescence image of secondary dendrites from (A). Golgi apparatus shown in magenta, Ykt6 in cyan; scale bar, 10µm. **D)** Fluorescence intensity linescans of the secondary dendrites from Box 2 in (A). **E)** Representative immunofluorescence image of Golgi apparatus (magenta) and Ykt6 (cyan) from Sh Ykt6-transduced primary hippocampal pyramidal neurons; scale bar, 10µm. **F)** Fluorescence intensity linescans of Golgi apparatus and Ykt6 from the soma (Box 1) in (E). **G)** Representative immunofluorescence image of secondary dendrites from (E). Golgi apparatus shown in magenta, Ykt6 in cyan; scale bar, 10µm. **H)** Fluorescence intensity linescans of the secondary dendrites from Box 2 in (E). **I-P)** Primary hippocampal pyramidal neurons were transduced with either Sh Ykt6 or Sh Ctrl at DIV5, induced for Ykt6 knockdown with doxycycline starting at DIV8 and immunostained at DIV21 with protein disulfide isomerase (PDI) (ER) and Ykt6. **I)** Representative immunofluorescence images of neurons transduced with Sh Ctrl of ER (magenta) and Ykt6 (cyan); scale bar, 10µm. **J)** Linescan of fluorescence intensities of ER and Ykt6 from the soma (Box 1) in (I). **K)** Representative immunofluorescence image of secondary dendrites from (I). ER shown in magenta, Ykt6 in cyan; scale bar, 10µm. **L)** Fluorescence intensity linescans of the secondary dendrites from Box 2 in (I). **M)** Representative immunofluorescence images of ER (magenta) and Ykt6 (cyan) from Sh Ykt6-transduced primary hippocampal pyramidal neurons. **N)** Linescan of fluorescence intensities of ER and Ykt6 from the soma (Box 1) in (M). **O)** Representative immunofluorescence images of secondary dendrites from (M). ER shown in magenta, Ykt6 in cyan ; scale bar, 10µm. **P)** Fluorescence intensity linescans of the secondary dendrites from Box 2 in (M).

Figure 3.

Ykt6 mobilizes to the postsynaptic spines in a cLTP-dependent manner. A) Left: representative images of secondary dendrites from primary pyramidal hippocampal neurons exposed to extracellular solution (ECS) as basal condition (top) or glycine for chemical long-term potentiation (cLTP, bottom) at DIV21 and immunostained with the postsynaptic marker, postsynaptic density 95 (PSD95) and Ykt6. Ykt6 in green, PSD95 in red. Scale bar, 5µm. Right: fluorescence intensity linescans from the region of interest (white box, left). (**B)** Quantification of average distance between PSD95 and Ykt6 from (A). Each data point represents aggregate average of all calculated shortest distances of each PSD95 puncta present in a selected ROI from a secondary dendrite to the closest Ykt6 puncta. N=2, 30-50 cells per biological replicate. Unpaired T-test. * $p \leq 0.05$. **C-E)** Adult rat brain tissue was exposed to cLTP or ECS, fractionated to cytosolic and synaptic fractions and immunoprobed for Ykt6, GluA1, GAPDH and PSD95; GAPDH serves as a loading control for the homogenate and the cytosolic fractions, and PSD95 serves as a loading control for the synaptosomal fraction. Representative western blot (C) with quantification over respective loading controls of Ykt6 (D) or GluA1 (E). N=3. Unpaired T-test. * $p \leq 0.05$.

Figure 4.

Ykt6 regulates GluA1 surface expression at synaptic spines in a cLTP-dependent manner. A) Representative western blot for Ykt6 expression from rat primary hippocampal neurons at DIV21, co-transduced with 3 different conditions: 1) Sh Ctrl + GFP, 2) Sh Ykt6 + GFP and 3) Sh Ykt6 + GFP-WT-Ykt6; solid arrow, endogenous Ykt6; dashed arrow, exogenous Ykt6. β-tubulin serves as a loading control. **B)** Quantification of Ykt6 endogenous expression over loading control from (A). **(C-D)** Rat primary hippocampal neurons co-transduced with 4 different conditions: 1) Sh Ctrl + GFP, 2) Sh Ctrl + GFP-WT-Ykt6, 3) Sh Ykt6 + GFP and 4) Sh Ykt6 + GFP-WT-Ykt6 were exposed to extracellular solution (ECS) or glycine for chemical long-term potentiation (cLTP) at DIV21 and immunolabelled for external and internal GluA1. **(C)** Representative immunofluorescence images of the secondary dendrites. Internal GluA1 in red, external GluA1 in green. Scale bar = 10µm. **(D)** Quantitation of ratios of external to internal GluA1 levels from (C), normalized to the control (basal condition, co-transduced with Sh Ctrl and GFP construct). One-way ANOVA with Welch's correction and Dunnett's multiple comparisons test. * $p \leq 0.05$, ** $p \leq 0.01$, *** $p \leq 0.001$, **** $p \leq 0.0001$. N=3, 8-10 cells per replicate.

Figure 5.

Ykt6 modulates both pre- and post-synaptic compartments of glutamatergic neurotransmission. Rat primary hippocampal pyramidal neurons were transduced with Sh Ctrl or Sh Ykt6 and patch-clamped in whole-cell configuration at DIV18-21 in the presence of tetrodotoxin (TTX), D-2-Amino-5-phosphonovalerate (D-APV), and picrotoxin (PTX) to isolate AMPA currents (A-D). **A)** Cumulative distribution of the amplitudes for all events per condition. **B)** Average amplitude per condition. **C)** Cumulative distribution of time between each event for every event per condition. **D)** Average frequency of events for each condition. ($p < 0.0001$, Kolmogorov-Smirnov test). **E)** Representative traces of cultures in (A); N=3, 4-6 cells per biological replicate. **F)** Quantitation of endogenous ATP levels at DIV21. N=3. **G)** Representative EM images of dendritic spines from the hippocampal cultures described above. **H)** Synaptic vesicle count for readily releasable pool (RRP). Each point is count for 1 image from (G). **I)** Synaptic vesicle count for recycling pool from (G). **J)** Synaptic vesicle count for reserve pool from (G). **K)** Average synaptic vesicle size from (G). All stats, Unpaired T-test with Welch's correction, * $p \leq 0.05$, ** $p \leq 0.01$, **** $p \leq 0.0001$.

Figure 6.

Dendritic arborization is dependent on Ykt6. Rat primary hippocampal neurons were transduced with either Sh Control or Sh Ykt6 RNA, transfected with PGK-mCherry construct on DIV19, immunoassayed for mCherry at DIV21 and analysed using Sholl analysis. **A)** Representative skeletonized images from pyramidal hippocampal neurons. **B)** Quantification of maximum number of intersections for hippocampal pyramidal neurons. **C)** Morphological analysis of hippocampal pyramidal neurons for the number of process intersections. Unpaired T-test with Welch's correction. * $p \leq 0.05$. N = 20-30, 10-15 cells per biological replicate. Scale bar: 100µm.

A

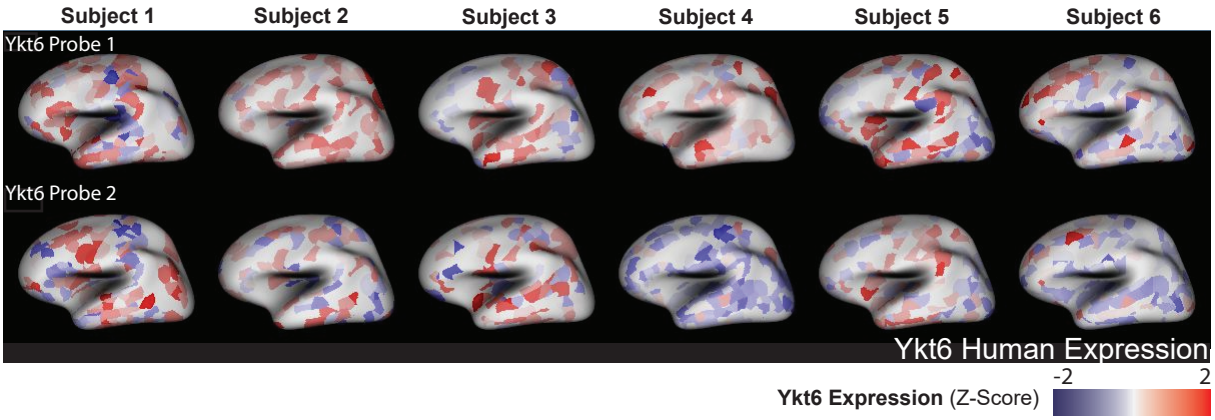
Subject 1
Subject 2
Subject 3
Subject 4
Subject 5
Subject 6
Ykt6 Probe 1
Ykt6 Probe 2
Ykt6 Human Expression
-2
2
Ykt6 Expression (Z-Score)

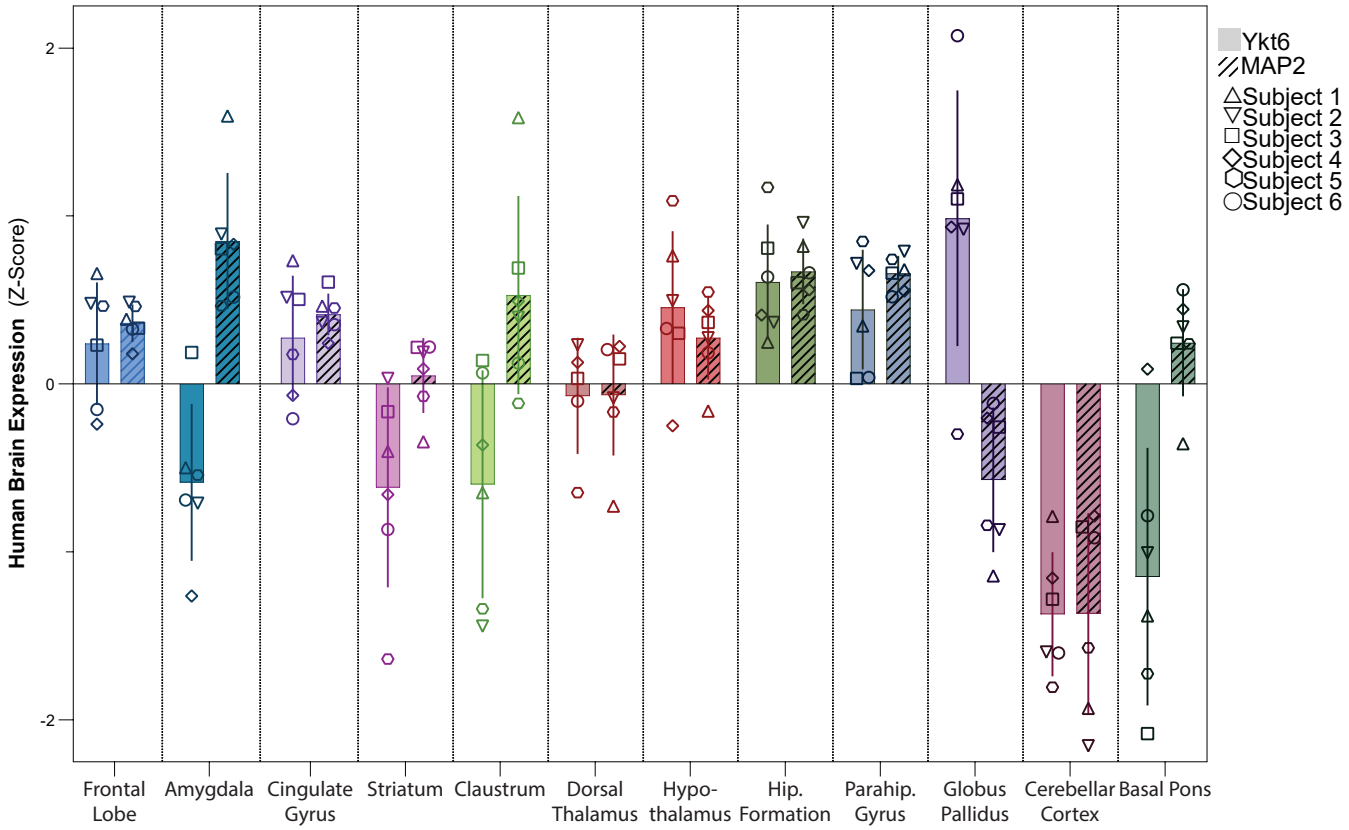
Human Brain Expression (Z-Score)
2
0
-2
Ykt6
MAP2
Subject 1
Subject 2
Subject 3
Subject 4
Subject 5
Subject 6
Frontal Lobe
Amygdala
Cingulate Gyrus
Striatum
Claustrum
Dorsal Thalamus
Hypo-thalamus
Hip. Formation
Parahip. Gyrus
Globus Pallidus
Cerebellar Cortex
Basal Pons

B

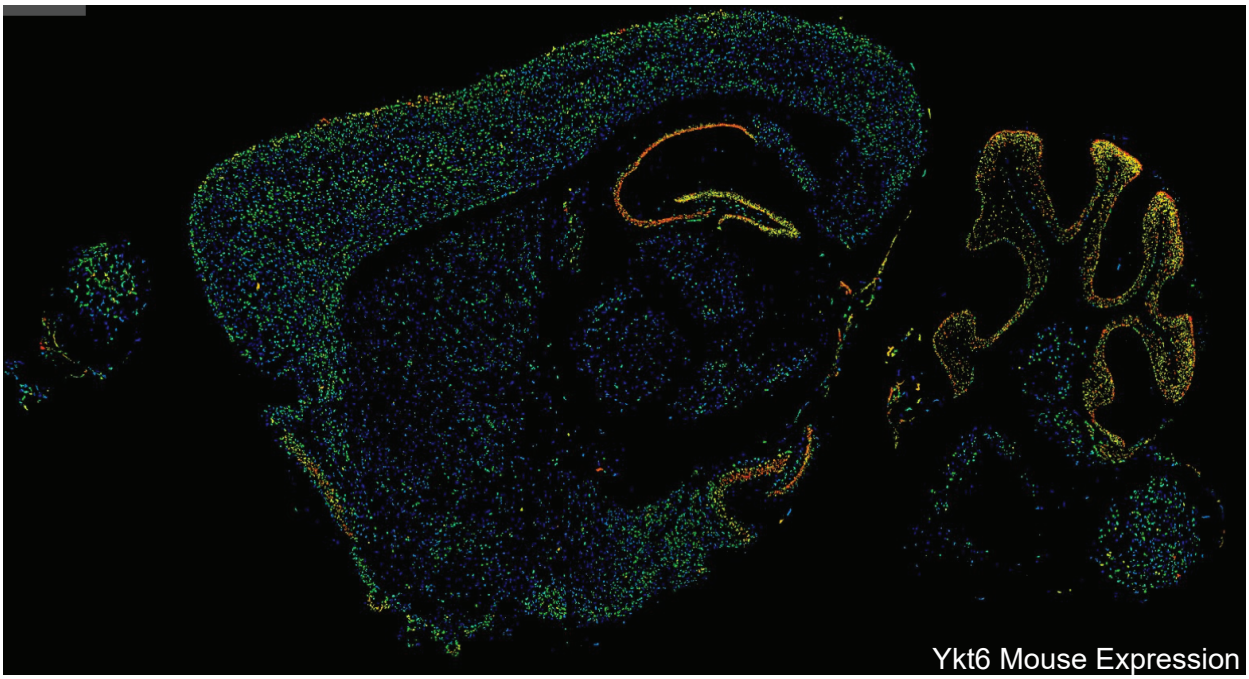
Ykt6 Mouse Expression

Figure 1.

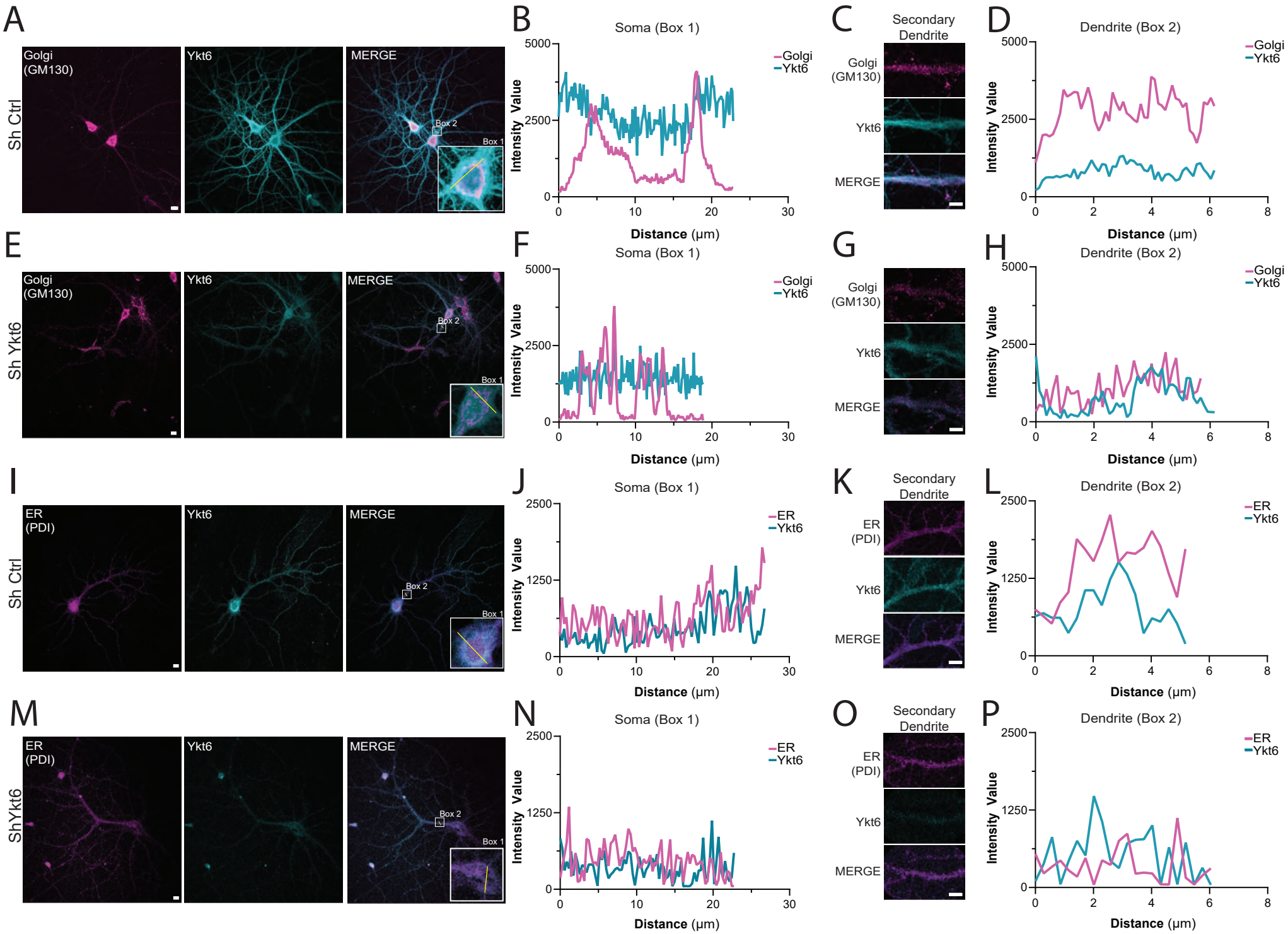
A
Sh Ctrl
Golgi (GM130)
Ykt6
MERGE
Box 2
Box 1
B
Soma (Box 1)
Golgi
Ykt6
Intensity Value
Distance (μm)
C
Secondary Dendrite
Golgi (GM130)
Ykt6
MERGE
D
Dendrite (Box 2)
Golgi
Ykt6
Intensity Value
Distance (μm)
E
Sh Ykt6
Golgi (GM130)
Ykt6
MERGE
Box 2
Box 1
F
Soma (Box 1)
Golgi
Ykt6
Intensity Value
Distance (μm)
G
Golgi (GM130)
Ykt6
MERGE
H
Dendrite (Box 2)
Golgi
Ykt6
Intensity Value
Distance (μm)
I
Sh Ctrl
ER (PDI)
Ykt6
MERGE
Box 2
Box 1
J
Soma (Box 1)
ER
Ykt6
Intensity Value
Distance (μm)
K
Secondary Dendrite
ER (PDI)
Ykt6
MERGE
L
Dendrite (Box 2)
ER
Ykt6
Intensity Value
Distance (μm)
M
ShYkt6
ER (PDI)
Ykt6
MERGE
Box 2
Box 1
N
Soma (Box 1)
ER
Ykt6
Intensity Value
Distance (μm)
O
Secondary Dendrite
ER (PDI)
Ykt6
MERGE
P
Dendrite (Box 2)
ER
Ykt6
Intensity Value
Distance (μm)

Figure 2.

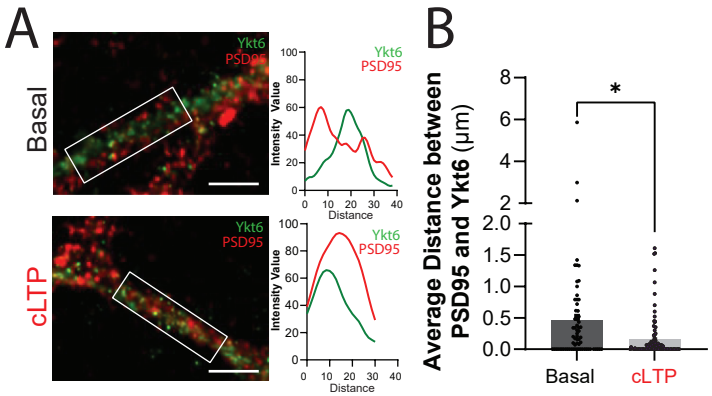
A
Basal
cLTP
Ykt6
PSD95
Intensity Value
Distance
B
Average Distance between PSD95 and Ykt6 (µm)
*
Basal
cLTP

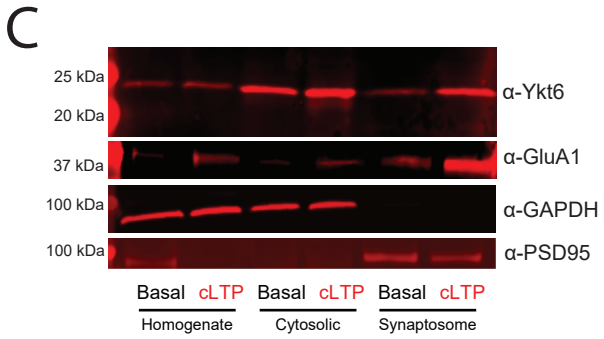
C
25 kDa
20 kDa
37 kDa
100 kDa
100 kDa
α-Ykt6
α-GluA1
α-GAPDH
α-PSD95
Basal cLTP Basal cLTP Basal cLTP
Homogenate
Cytosolic
Synaptosome

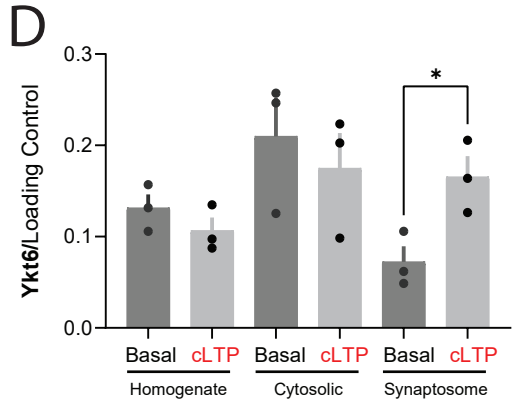
D
Ykt6/Loading Control
*
Basal cLTP Basal cLTP Basal cLTP
Homogenate
Cytosolic
Synaptosome

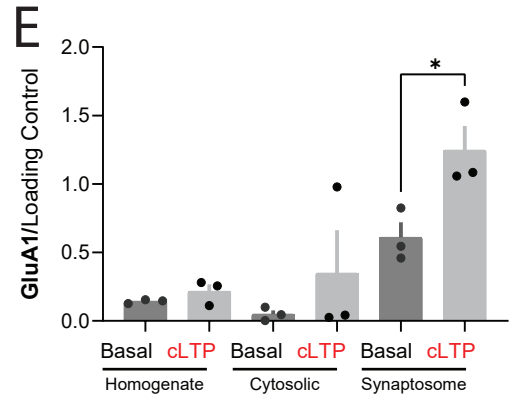
E
GluA1/Loading Control
*
Basal cLTP Basal cLTP Basal cLTP
Homogenate
Cytosolic
Synaptosome

Figure 3.

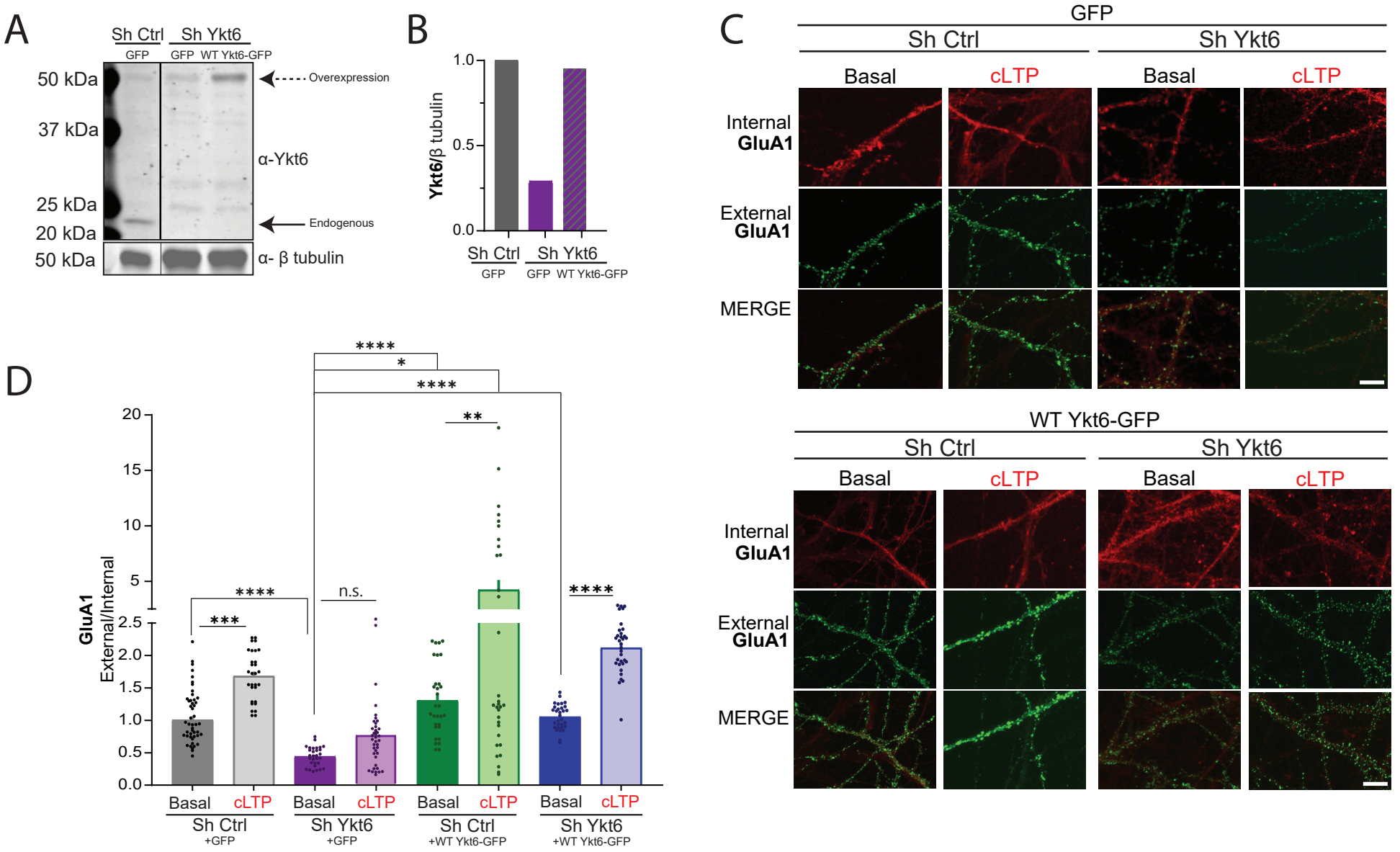
A
Sh Ctrl
Sh Ykt6
GFP
GFP
WT Ykt6-GFP
50 kDa
37 kDa
25 kDa
20 kDa
50 kDa
Overexpression
α-Ykt6
Endogenous
α- β tubulin
B
Ykt6/β tubulin
1.0
0.5
0.0
Sh Ctrl
Sh Ykt6
GFP
GFP
WT Ykt6-GFP
C
GFP
Sh Ctrl
Sh Ykt6
Basal
cLTP
Basal
cLTP
Internal GluA1
External GluA1
MERGE
WT Ykt6-GFP
Sh Ctrl
Sh Ykt6
Basal
cLTP
Basal
cLTP
Internal GluA1
External GluA1
MERGE
D
GluA1 External/Internal
20
15
10
5
2.5
2.0
1.5
1.0
0.5
0.0
****
*
****
**
****
***
n.s.
****
Basal
cLTP
Basal
cLTP
Basal
cLTP
Basal
cLTP
Sh Ctrl +GFP
Sh Ykt6 +GFP
Sh Ctrl +WT Ykt6-GFP
Sh Ykt6 +WT Ykt6-GFP

Figure 4.

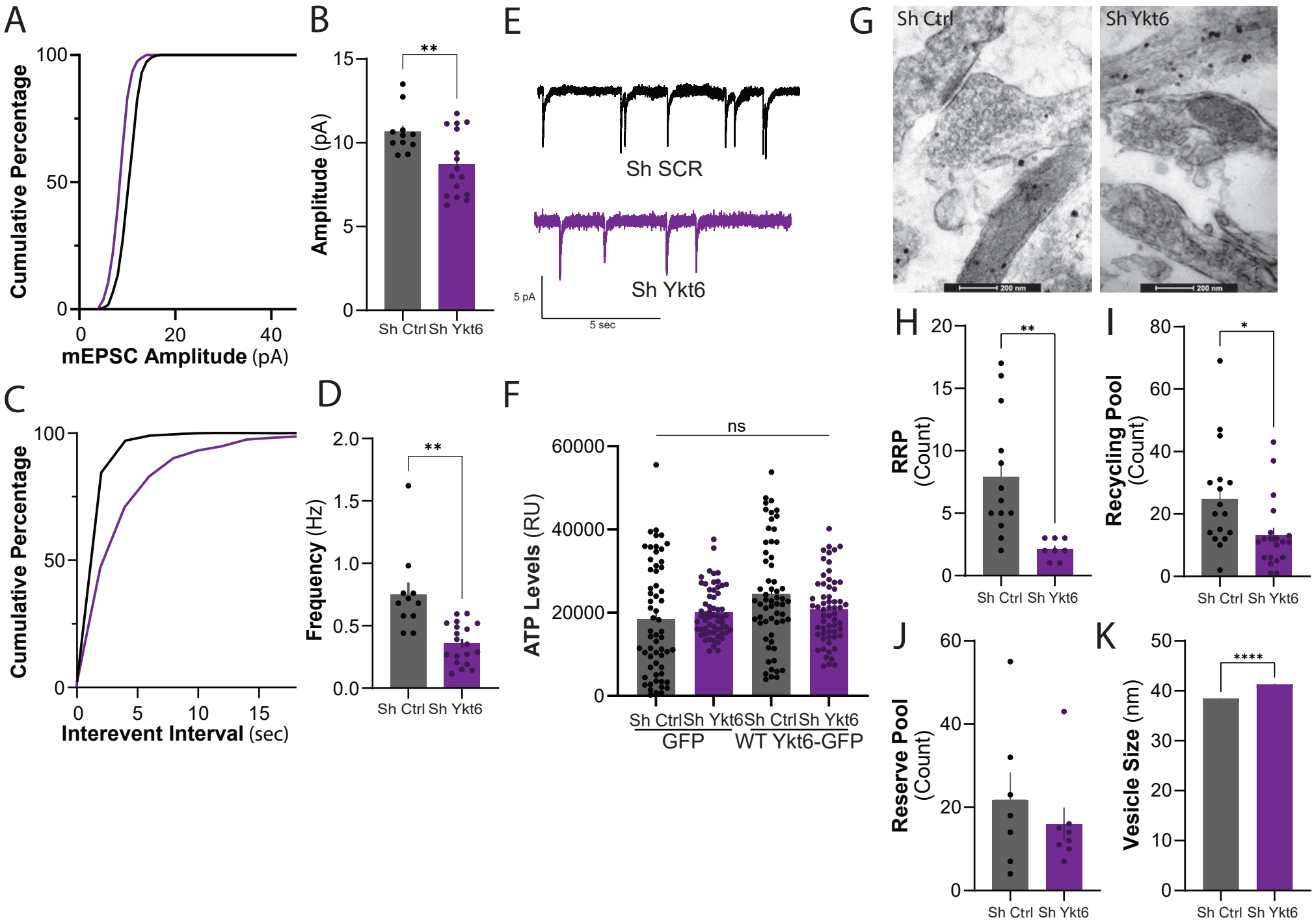
A
Cumulative Percentage
100
50
0
0
20
40
mEPSC Amplitude (pA)
B
Amplitude (pA)
15
10
5
0
**
Sh Ctrl
Sh Ykt6
E
Sh SCR
Sh Ykt6
5 pA
5 sec
G
Sh Ctrl
Sh Ykt6
200 nm
200 nm
C
Cumulative Percentage
100
50
0
0
5
10
15
Interevent Interval (sec)
D
Frequency (Hz)
2.0
1.5
1.0
0.5
0.0
**
Sh Ctrl
Sh Ykt6
F
ATP Levels (RU)
60000
40000
20000
0
ns
Sh Ctrl
Sh Ykt6
Sh Ctrl
Sh Ykt6
GFP
WT Ykt6-GFP
H
RRP (Count)
20
15
10
5
0
**
Sh Ctrl
Sh Ykt6
I
Recycling Pool (Count)
80
60
40
20
0
*
Sh Ctrl
Sh Ykt6
J
Reserve Pool (Count)
60
40
20
0
Sh Ctrl
Sh Ykt6
K
Vesicle Size (nm)
50
40
30
20
10
0
****
Sh Ctrl
Sh Ykt6

Figure 5.

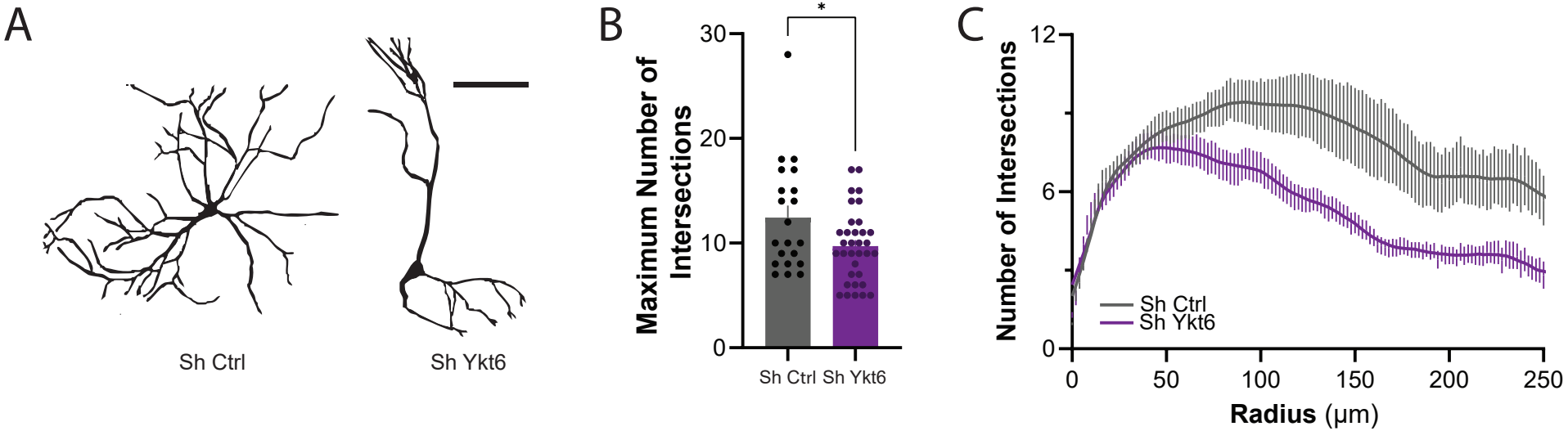
A
Sh Ctrl
Sh Ykt6
B
Maximum Number of Intersections
30
20
10
0
*
Sh Ctrl
Sh Ykt6
C
Number of Intersections
12
6
0
Sh Ctrl
Sh Ykt6
0
50
100
150
200
250
Radius (μm)

Figure 6.